I&EC research
Industrial & Engineering Chemistry Research

pubs.acs.org/IECR
Article

CO_2-Driven pH Control in the Enzymatic Hydrolysis of Urea: Stochastic Model Predictive Control under Uncertainty

Published as part of Industrial & Engineering Chemistry Research special issue "Smart Reactors - Towards Adaptive, Resilient, and Autonomous Process Systems".

Srimanta Santra,* Leandros Paschalidis, Mirko Skiborowski, and Timm Faulwasser*

Cite This: *Ind. Eng. Chem. Res.* 2026, 65, 15071−15088

ABSTRACT: Enzymatic urea hydrolysis is a mild route to ammonia production, but urease activity is strongly pH dependent. In buffer-free operation, pH can drift substantially because ammonia and inorganic carbon rapidly repartition through acid−base equilibria. Detailed process-modeling background, experimental protocol, and parameter identification context are reported in a companion manuscript by Dittmer, K. R. (2026). Here, in contrast, we develop an uncertainty-aware modeling and control framework for CO_2-driven pH regulation during urease-catalyzed urea hydrolysis. A control-oriented mechanistic model couples pH-dependent urease kinetics with substrate and product inhibition, fast speciation with electroneutrality-based pH computation, and gas−liquid mass transfer of NH_3 and CO_2 in a headspace. Parametric uncertainty in kinetic and transfer parameters is propagated using nonintrusive polynomial chaos expansion. Building on these predictions, we propose a stochastic model predictive control (SMPC) scheme that tracks a pH reference under input constraints while enforcing chance constraints on pH safety bounds. Simulations demonstrate uncertainty-aware pH regulation without buffer salts under the considered parametric uncertainty scenarios, providing a foundation for automated operation of enzymatic reactors under uncertainty.

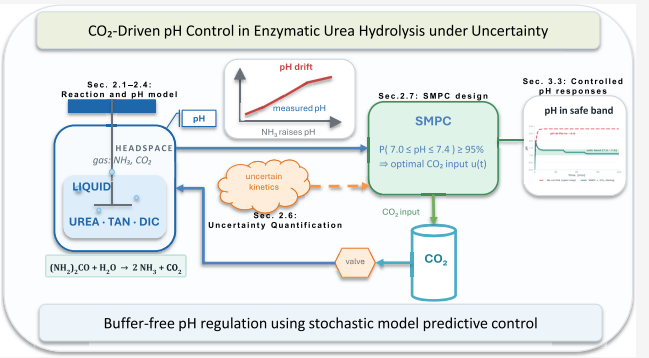

1. INTRODUCTION

Enzymatic biotransformations enable chemical production under mild conditions and can reduce energy demand and hazardous byproducts compared with conventional routes. Their performance, however, is often highly sensitive to operating conditions such as temperature and pH. A prominent example is urease catalyzed urea hydrolysis, which converts urea into ammonia and carbon dioxide and is relevant to mild-condition ammonia production, wastewater treatment, and urea removal and recovery processes.[2−6]

A central challenge is that urease activity is strongly pH dependent, with a narrow optimal window near neutral pH. In buffer-free media, urea hydrolysis continuously alters total ammonia nitrogen (TAN) and dissolved inorganic carbon (DIC). Because acid−base reactions are fast, TAN and DIC rapidly repartition among ammonia and carbonate species, and the resulting charge balance can drive pronounced pH drift. These excursions reduce enzyme activity and lead to inconsistent conversion and productivity. Conventional pH control relies on buffer salts or strong acid base addition, but this increases salt load and can complicate downstream processing, which motivates buffer-free alternatives.

CO_2 dosing provides a clean pH actuator in buffer-free operation. Dissolved CO_2 increases the inorganic carbon pool and, through carbonate equilibria, counteracts alkalinization induced by ammonia formation. Importantly, the manipulated CO_2 input affects pH through a transport pathway: gas−liquid mass transfer determines how quickly CO_2 is absorbed and how strongly it can reshape the carbonate system. As a result, pH regulation must account for the coupled effect of (i) pH dependent urease kinetics, (ii) fast speciation and electroneutrality based pH computation, and (iii) gas−liquid exchange. In addition, key parameters vary across experiments due to biological variability in effective enzyme activity and uncertainty in mass transfer conditions, which can substantially broaden the pH trajectory and complicate control design.

Received: March 5, 2026
Revised: June 19, 2026
Accepted: June 19, 2026
Published: July 9, 2026

https://doi.org/10.1021/acs.iecr.6c01013
Ind. Eng. Chem. Res. 2026, 65, 15071−15088

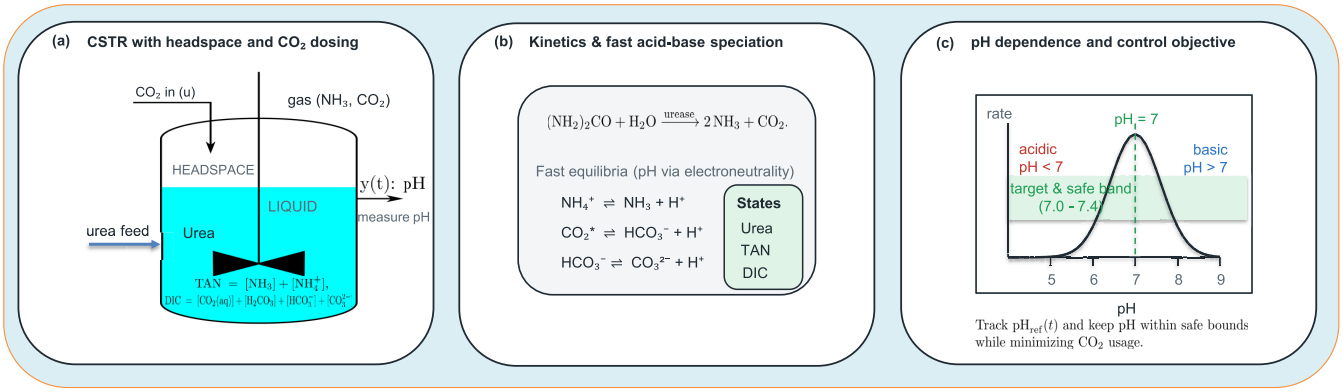

Figure 1. Overview of buffer-free pH regulation for urease-catalyzed urea hydrolysis using CO_2 dosing and stochastic MPC. (a) Well-mixed stirred batch reactor with a gas headspace. The manipulated input $u(t)$ is the CO_2 molar feed rate to the headspace; through gas−liquid mass transfer it adjusts the dissolved inorganic carbon pool, and the resulting pH is measured in the liquid phase. The dynamic state vector consists of the total species UREA, TAN, and DIC together with the gas-phase inventories. (b) Urease kinetics and fast acid−base equilibria used for pH computation via electroneutrality. (c) Illustration of the pH dependence of urease activity and the control objective: track $pH_{ref}(t)$ while enforcing the probabilistic safety bounds [7.0, 7.4] and minimizing CO_2 usage.

Prior work has established pH dependent urease rate laws and highlighted the strong feedback between pH and reaction rate.[7,8] Carbonate system modeling and TAN and DIC bookkeeping are standard in aquatic and wastewater chemistry,[9−11] and gas−liquid exchange is commonly described via Henry's law with linear driving force transfer.[12−14] While these components provide a sound modeling basis, uncertainty-aware pH control remains challenging because pH is obtained from a nonlinear charge balance relation and because both kinetic and transfer parameters are uncertain.

The present paper focuses on the uncertainty and control-related aspects of CO_2 driven pH regulation in buffer-free urea hydrolysis. The basis of our work is the process-focused study presented in the companion paper by Dittmer et al.,[1] which provides the detailed modeling background, experimental protocol, and parameter-identification context for the urea-hydrolysis system. In contrast, here we consider uncertainty-aware control of urea hydrolysis using polynomial chaos expansions (PCE) in an MPC framework. To this end, we consider a compact, control-oriented lower-complexity model that includes only the elements required for uncertainty propagation and controller synthesis. An overview of the overall setup and control objective is given in Figure 1. We emphasize that PCE and chance-constrained stochastic MPC are established tools. Hence, the main purpose of this work is not the introduction of novel PCE or SMPC algorithms. Rather, our contribution is to formulate and evaluate an uncertainty-aware control framework for CO_2-driven pH regulation in buffer-free enzymatic urea hydrolysis. This setting is challenging because pH is obtained from nonlinear electroneutrality-based acid−base speciation, CO_2 acts indirectly through gas−liquid mass transfer and carbonate equilibria, and the urease rate depends strongly on the resulting pH. The novelty of the present work is therefore the integration of reaction, speciation, transport, uncertainty propagation, and receding-horizon control within a control-oriented reactor framework. More broadly, the study shows how SMPC can be formulated when the controlled variable is an algebraic chemical equilibrium output rather than a directly integrated state, and when the manipulated input acts indirectly through gas−liquid transfer. These features arise in many reactive pH control problems and are not specific to urea hydrolysis alone.

Our main contributions are as follows:

- We develop a control-oriented reactor model that couples urea hydrolysis to pH through TAN and DIC mass balances, fast acid−base speciation, and gas−liquid CO_2 mass transfer. The model retains the dominant uncertainty mechanisms in kinetics and transport while remaining simple enough for online uncertainty propagation and controller synthesis.
- We use nonintrusive polynomial chaos expansion (PCE) to propagate uncertainty through the coupled ODE−DAE reactor model, including the nonlinear electroneutrality-based pH calculation, and thereby obtain time-resolved pH statistics for controller design.
- We formulate a stochastic model predictive controller (SMPC) for CO_2 dosing in which pH constraints are imposed probabilistically on an algebraic speciation output, while the manipulated input acts indirectly through gas−liquid transfer and carbonate equilibria.

The remainder of the paper is organized as follows. Section 2 introduces the reaction system and the problem formulation. Section 2.5 summarizes the control-oriented reactor model adopted from the companion manuscript.[1] The kinetic model choices (Qin-type versus companion kinetics) and the resulting model-mismatch setup are described in Remark 1. Section 2.6 introduces the parametric uncertainty description and Section 2.6.1 presents the nonintrusive PCE used for uncertainty propagation. Section 2.7 formulates the SMPC scheme for CO_2-driven pH regulation. Simulation results are reported in Section 3, followed by conclusions in Section 4.

2. PROBLEM AND METHOD

In enzymatic urea hydrolysis, urease activity is strongly pH dependent, so process performance is sensitive to how well pH is maintained near the enzyme's optimal range. A common way to stabilize pH is to add buffer salts or strong acid or base, but this increases salt load, can raise operating cost, and may complicate downstream processing. In buffer-free operation, urea hydrolysis generates total ammonia nitrogen (TAN) and dissolved inorganic carbon (DIC). Fast acid−base equilibria redistribute these conserved totals among ammonia and carbonate species, often driving substantial pH drift. Because pH is obtained from a

https://doi.org/10.1021/acs.iecr.6c01013
Ind. Eng. Chem. Res. 2026, 65, 15071−15088

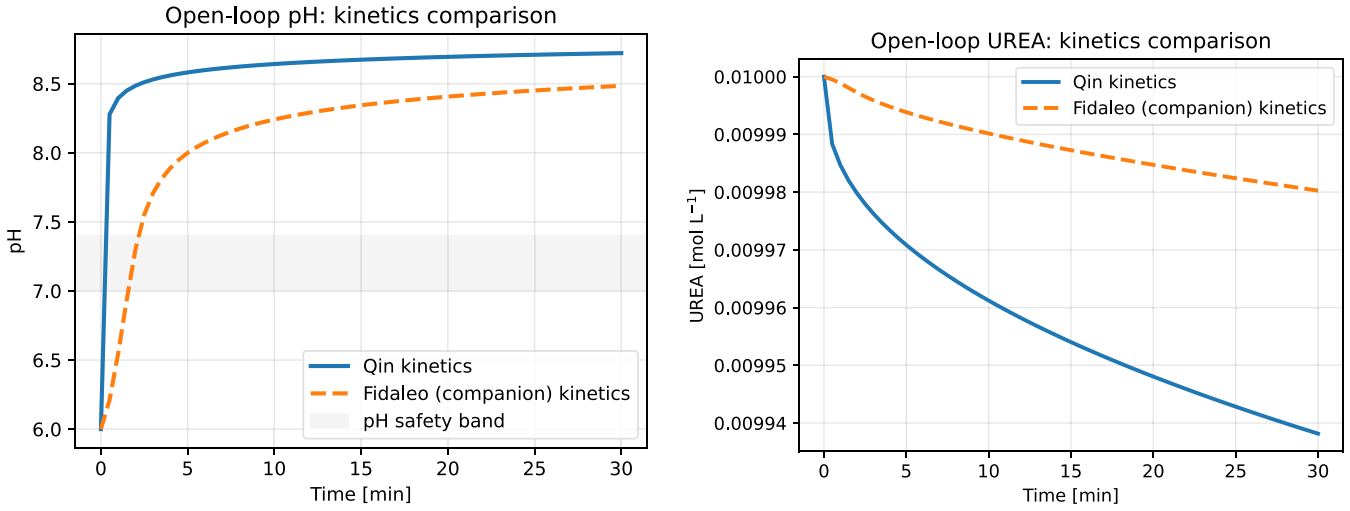

(a) Open-loop pH. (b) Open-loop UREA concentration.

Figure 2. Open-loop sensitivity of the predicted pH and UREA trajectories to the kinetic model form (a, b). The Qin-type kinetic law[7] is compared with the companion kinetic law.[1] In this comparison, only the urease kinetic rate expression is changed, while the reactor balances, acid−base speciation and electroneutrality calculation, gas−liquid mass-transfer model, initial conditions, temperature, and operating conditions are kept fixed. Thus, the differences between the curves isolate the effect of kinetic model-form choice.

nonlinear charge-balance relation, even moderate variability in kinetics or mass transfer can cause large changes in pH.

To regulate pH without buffer salts, we use CO_2 dosing as a clean actuator. CO_2 transfers from the gas phase into the liquid and increases the effective inorganic carbon pool, which shifts carbonate speciation and lowers pH. This introduces an actuator pathway governed by gas−liquid mass transfer and therefore an intrinsic lag between the manipulated CO_2 input and the pH response. Moreover, key parameters are uncertain in practice, including effective enzyme kinetics, gas−liquid mass-transfer coefficients, and solubility parameters. The goal of this work is to propagate these uncertainties and design a stochastic MPC scheme that selects CO_2 dosing to track a desired pH reference while respecting input bounds and probabilistic pH safety constraints.

In this work, we focus on uncertainty-aware pH regulation via CO_2 dosing and the associated stochastic MPC design. Here we provide the complete control-oriented model structure used for uncertainty propagation and closed-loop SMPC design. The companion manuscript[1] provides the detailed experimental procedures, parameter-identification study, and additional process-modeling background. This organization makes the present manuscript self-contained with respect to the model equations used in the controller, while avoiding duplication of the full experimental study.

2.1. Enzymatic Urea Hydrolysis

Urease catalyzes the hydrolysis of urea and is widely studied in enzymology and bioprocess settings.[2,3,5,6] At the level of overall stoichiometry, the reaction is

$$(NH_2)_2CO + H_2O \xrightarrow{\text{urease}} 2NH_3 + CO_2 \quad (1)$$

In buffer-free operation, the products do not remain solely as molecular NH_3 and CO_2. Instead, they rapidly redistribute through acid−base equilibria, which drives the strong and often fast pH changes observed in urea−urease systems.[7,8,10] Rather than tracking every ionic species dynamically, we keep the slow mass balances in terms of conserved totals and compute speciation algebraically. Specifically, we use

$$TAN = [NH_3] + [NH_4^+],$$

$$DIC = [CO_2^*] + [HCO_3^-] + [CO_3^{2-}]$$

where $CO_2^* = CO_2(aq) + H_2CO_3$.

Neglecting gas−liquid transfer and assuming a well-mixed liquid phase with no side reactions, each mole of urea consumed produces two moles of TAN and one mole of DIC by 1. In differential form

$$\frac{dTAN}{dt} = 2r_u(t), \qquad \frac{dDIC}{dt} = r_u(t), \quad (2)$$

where $r_u(t)$ is the urea consumption rate and $d\,UREA/dt = -r_u(t)$. In the full reactor model below, TAN and DIC change due to both enzymatic reaction and gas−liquid exchange, while the internal partitioning among conjugate acid−base pairs is treated as instantaneous equilibrium. At each time point, pH and the volatile species concentrations, in particular $[NH_3]$ and $[CO_2^*]$, are recovered from TAN and DIC by solving the equilibrium and electroneutrality relations. This separation keeps the dynamic model compact and control-oriented while still capturing the key pH feedback created by fast speciation.

Sections 2.2−2.5 summarize the complete control-oriented model used in the present SMPC study. Detailed experimental procedures, parameter estimation, and additional process-modeling details are provided in the companion manuscript.[1]

2.2. Kinetic Model

Buffer-free urea hydrolysis exhibits strong coupling between pH and enzymatic activity, so the kinetic law must explicitly depend on pH.[7,8] We adopt the extended Michaelis−Menten type expression of Qin and Cabral,[7] which accounts for temperature dependence, a pH activity window, substrate inhibition, and product inhibition. The full kinetic parametrization and process-modeling context are discussed in the companion manuscript.[1] Here we state the rate law and definitions required for the stochastic MPC formulation.

https://doi.org/10.1021/acs.iecr.6c01013
Ind. Eng. Chem. Res. 2026, 65, 15071−15088

We employ the Qin-type kinetic law as a control-oriented baseline. Its smooth low-order structure supports stable PCE moment propagation and numerically robust SMPC over the finite prediction horizon. The proposed SMPC framework is not tied to this specific kinetic form. Rather, the Qin-type model provides a consistent baseline for uncertainty-aware control design, while the impact of alternative kinetics is assessed through the model-form comparison in Remark 1 and Figure 2.

Let C_E denote the urease loading in $g_{urease}L^{-1}$. The volumetric ammonia production rate is

$$r_{NH_3}(t) = C_E \nu_{NH_3}(T(t), \mathrm{pH}(t), [\mathrm{UREA}](t), [NH_3](t)) \quad (\mathrm{mol}NH_3L^{-1}s^{-1}), \tag{3}$$

where ν_{NH_3} is the specific ammonia formation rate in mol NH_3 s^{-1} g_{urease}^{-1}. We model ν_{NH_3} as

$$\nu_{NH_3}(T, \mathrm{pH}, [S], [P]) = k_0 \exp\left(-\frac{E_a}{RT}\right) \frac{1}{f_{\mathrm{pH}}(\mathrm{pH}) f_S([S]) f_P([P], \mathrm{pH})} \tag{4}$$

with

$$f_{\mathrm{pH}}(\mathrm{pH}) = 1 + \left(\frac{K_{es,1}}{[H^+]}\right)^{\alpha} + \left(\frac{[H^+]}{K_{es,2}}\right)^{\beta},$$
$$f_S([S]) = 1 + \frac{K_M}{[S]} + \frac{[S]}{K_S},$$
$$f_P([P], \mathrm{pH}) = 1 + \frac{[P]}{K_p(\mathrm{pH})} \tag{5}$$

Here, $[S] = [\mathrm{UREA}]$ is the urea concentration, $[H^+] = 10^{-\mathrm{pH}}$ is the hydrogen ion concentration, and $[P] = [NH_3]$ is the molecular ammonia concentration. In the reactor model, $[NH_3]$ is obtained from TAN speciation at the current pH.

Since one mole of urea produces two moles of ammonia, the urea consumption rate used in the conserved total balances is

$$r_u(t) = \frac{1}{2} r_{NH_3}(t) \quad (\mathrm{mol\ UREA}L^{-1}\,s^{-1}) \tag{6}$$

We treat $r_u(t)$ as a positive consumption rate and apply it with the appropriate sign in the material balances.

To clarify the comparison in Figure 2, "model-form sensitivity" refers here to changing only the urease kinetic law while keeping all other model components fixed. Specifically, the reactor balances, acid–base speciation and electroneutrality calculation, gas–liquid mass-transfer model, initial conditions, temperature, and operating conditions are identical in both simulations. Therefore, the differences in the predicted pH and UREA trajectories isolate the effect of kinetic model-form choice.

2.3. Acid–Base Equilibrium Model

The reactor pH is computed from the conserved totals TAN and DIC using equilibrium speciation and an electroneutrality closure, following standard practice in aquatic and wastewater chemistry.[9−11] At each time t, we solve the charge-balance equation for $H(t) = [H^+](t)$ and set

$$\mathrm{pH}(t) = -\log_{10}(H(t))$$

For given TAN and DIC, the species concentrations are expressed as functions of H through equilibrium speciation fractions. The charge-balance relation is

$$H + [NH_4^+] = [OH^-] + [HCO_3^-] + 2[CO_3^{2-}] \tag{7}$$

The molecular species concentrations needed for gas–liquid transfer and kinetic inhibition are then obtained as

$$[NH_3](t) = \alpha_{NH_3}(\mathrm{H}(t), T(t))\mathrm{TAN}(t) \tag{8}$$

$$[CO_2^*](t) = \alpha_{CO_2^*}(\mathrm{H}(t), T(t))\mathrm{DIC}(t) \tag{9}$$

The full equilibrium parametrization and temperature-dependent constants are given in the companion manuscript.[1] In the present work, this algebraic pH calculation closes the coupling between reaction, speciation, gas–liquid transfer, and control.

2.4. Gas–Liquid Mass-Transfer Model

CO_2 dosing affects pH through gas–liquid transfer into the dissolved CO_2^* pool followed by fast carbonate speciation. Conversely, only molecular NH_3 is volatile and can be stripped to the headspace.[12−14] The headspace is modeled as an ideal gas mixture in a fixed gas volume V_{gas} at temperature T. For $i \in \{NH_3, CO_2\}$, the partial pressure is computed from gas-phase moles $n_{i,g}$ via

$$P_i(t) = \frac{n_{i,g}(t)RT}{V_{gas}} \tag{10}$$

where R is the universal gas constant.

Gas–liquid exchange is described by a linear driving-force model with volumetric mass-transfer coefficient $k_L a_i$

$$r_{i,\mathrm{tr}}(t) = k_L a_i (C_{i,l}(t) - C_{i,l}^*(t)), \quad C_{i,l}^*(t) = H_i P_i(t) \tag{11}$$

where $C_{i,l}$ is the bulk dissolved concentration, $C_{i,l}^*$ is the equilibrium dissolved concentration corresponding to the gas partial pressure, and H_i is Henry's law constant. For ammonia, $C_{i,l} = [NH_3]$, while for carbon dioxide, $C_{i,l} = [CO_2^*]$.

The transfer rates enter the liquid-phase total balances as

$$\frac{\mathrm{dTAN}}{\mathrm{d}t} = 2r_u(t) - r_{NH_3,\mathrm{tr}}(t) \tag{12}$$

$$\frac{\mathrm{dDIC}}{\mathrm{d}t} = r_u(t) - r_{CO_2,\mathrm{tr}}(t) \tag{13}$$

and the gas-phase inventories evolve as

$$\frac{\mathrm{d}n_{NH_3,g}}{\mathrm{d}t} = V_l r_{NH_3,\mathrm{tr}}(t) \tag{14}$$

$$\frac{\mathrm{d}n_{CO_2,g}}{\mathrm{d}t} = V_l r_{CO_2,\mathrm{tr}}(t) + \dot{n}_{CO_2,\mathrm{supply}}(t) \tag{15}$$

where V_l is the liquid volume and $\dot{n}_{CO_2,\mathrm{supply}}(t)$ is the externally supplied CO_2 molar flow rate used as the manipulated input in the SMPC formulation.

2.5. Control-Oriented Model

The control-oriented reactor model used in this work is summarized below so that the SMPC formulation can be followed without consulting the companion manuscript. The model consists of conserved total balances for UREA, TAN, and DIC, gas-phase balances for NH_3 and CO_2, gas–liquid mass transfer, and an algebraic acid–base, electroneutrality calcu-

https://doi.org/10.1021/acs.iecr.6c01013
Ind. Eng. Chem. Res. 2026, 65, 15071−15088

Table 1. Control-Oriented Model Components Used in the SMPC Study

component	description	role
UREA balance	urea is consumed by urease-catalyzed hydrolysis.	reaction progress.
TAN balance	TAN increases through ammonia production and changes through NH_3 gas−liquid transfer.	alkaline contribution to pH.
DIC balance	DIC increases through CO_2 formation and changes through CO_2 gas−liquid transfer and dosing.	carbonate contribution to pH.
gas-phase balances	NH_3 and CO_2 inventories determine headspace partial pressures.	gas−liquid coupling and actuation.
acid−base speciation	TAN and DIC are mapped to molecular and ionic species through equilibrium fractions.	algebraic pH calculation.
electroneutrality closure	the hydronium concentration $H = [H^+]$ is obtained by solving the charge-balance equation.	defines $pH = -\log_{10}H$.
urease kinetics	the rate depends on UREA, pH, temperature, substrate inhibition, and product inhibition.	nonlinear reaction source term.
uncertain parameters	kinetic, enzyme-loading, mass-transfer, and solubility parameters are treated as uncertain.	propagated by PCE.

lation for pH. The companion manuscript[1] provides the full experimental protocols, parameter estimation details, and additional process modeling background. Here, we state the equations, assumptions, state variables, inputs, and uncertain parameters that are used directly in the uncertainty propagation and SMPC simulations.

We consider a well mixed[15,16] liquid volume V_l with a headspace volume V_{gas} at temperature T. Liquid volume and temperature are taken as known constant or prescribed. The dynamic states are

$$x(t) = [\mathrm{UREA}(t),\ \mathrm{TAN}(t),\ \mathrm{DIC}(t),\ n_{\mathrm{NH_3,g}}(t),\ n_{\mathrm{CO_2,g}}(t)]^\tau \tag{16}$$

where UREA, TAN, and DIC denote liquid-phase concentrations in mol L^{-1}, and $n_{i,g}$ denotes the gas-phase amount of species i in mol. The manipulated input is the CO_2 molar feed rate $u(t) = \dot{n}_{\mathrm{CO_2,supply}}(t)$(mol s^{-1}). The control-oriented reactor model combines (i) urea hydrolysis kinetics, (ii) instantaneous acid−base speciation used to compute pH, and (iii) finite rate gas−liquid mass transfer in a headspace. We can now summarize the coupled gas−liquid dynamics in terms of conserved totals and gas phase inventories

$$r_{\mathrm{NH_3}}(t) = C_E \nu_{\mathrm{NH_3}}(\mathrm{UREA}(t),\ \mathrm{pH}(t),\ T(t)) \tag{17}$$

$$r_u(t) = \frac{1}{2} r_{\mathrm{NH_3}}(t) \tag{18}$$

$$[\mathrm{NH_3}](t) = \alpha_{\mathrm{NH_3}}(H(t),\ T(t))\mathrm{TAN}(t) \tag{19}$$

$$[\mathrm{CO_2^*}](t) = \alpha_{\mathrm{CO_2^*}}(H(t),\ T(t))\mathrm{DIC}(t) \tag{20}$$

$$r_{\mathrm{NH_3,tr}} = k_L a_{\mathrm{NH_3}}([\mathrm{NH_3}] - H_{\mathrm{NH_3}} P_{\mathrm{NH_3}}) \tag{21}$$

$$r_{\mathrm{CO_2,tr}} = k_L a_{\mathrm{CO_2}}([\mathrm{CO_2^*}] - H_{\mathrm{CO_2}} P_{\mathrm{CO_2}}) \tag{22}$$

$$\frac{\mathrm{dUREA}}{\mathrm{d}t} = -r_u \tag{23}$$

$$\frac{\mathrm{dTAN}}{\mathrm{d}t} = 2r_u - r_{\mathrm{NH_3,tr}} \tag{24}$$

$$\frac{\mathrm{dDIC}}{\mathrm{d}t} = r_u - r_{\mathrm{CO_2,tr}} \tag{25}$$

$$\frac{\mathrm{d}n_{\mathrm{NH_3},g}}{\mathrm{d}t} = V_l r_{\mathrm{NH_3,tr}} \tag{26}$$

$$\frac{\mathrm{d}n_{\mathrm{CO_2},g}}{\mathrm{d}t} = V_l r_{\mathrm{CO_2,tr}} + u(t) \tag{27}$$

Specifically, 17 and 18 define the volumetric reaction rate, 19 and 20 map totals to volatile molecular species through speciation fractions, and 21 and 22 define the interphase transfer rates.

The manipulated input is the CO_2 supply rate $u(t)$ entering the headspace balance in 27. The reaction rate depends on pH through $\nu_{\mathrm{NH3}}(\cdot)$, where pH is obtained at each time from the electroneutrality closure in1 by solving for $H(t) = [H^+](t)$ and setting $\mathrm{pH(t)} = -\log_{10}(H(t))$. Together, the dynamic balances in eqs 17−27 and the algebraic speciation relations form the differential−algebraic prediction model that is used both for uncertainty propagation and for the proposed SMPC design. The main components of the control-oriented model used in the SMPC study are in Table 1.

The urease kinetic law is stated explicitly because it is central to both the uncertainty propagation and the structural model-mismatch study. We use the Qin-type kinetics[7] as a literature baseline for controller synthesis and then test the controller against the alternative kinetic law reported in the companion manuscript.[1] The reactor balances, acid−base closure, and gas−liquid transfer model are summarized above so that the prediction model used for SMPC is self-contained.

Remark 1 *The SMPC formulation in this work uses the Qin-type pH dependent kinetics.*[7] *In the companion modeling and experimental manuscript,*[1] *an alternative kinetic law is used because the experimentally observed pH dependence of urease activity was stronger than predicted by the Qin-type model. To illustrate the impact of this modeling choice while holding all other model components fixed, we compare open-loop predictions in* Figure 2. *The kinetic law changes both the pH drift time scale in* Figure 2a *and the predicted UREA concentration profile in* Figure 2b. *Nevertheless, as our results in* Section 3 *show, the Qin-type model can be employed for uncertainty-aware control design.*

2.6. Nonintrusive Model-Based Uncertainty Quantification

The considered uncertainties have direct physical origins in the experimental system. First, urease is a biological catalyst and its effective activity varies between preparations and runs due to batch-to-batch variability, storage history, and possible slow deactivation during the experiment. This variability is represented through uncertainty in the effective kinetic scale k_0 and the effective enzyme loading C_E. When kinetic parameters are estimated from data at a finite number of temperatures, the activation energy E_a also becomes uncertain. Second, the apparent saturation and inhibition constants K_M, K_S are effective parameters that depend on the local chemical environment pH, ionic strength, and are typically identified from limited data, which introduces uncertainty. Third, gas−liquid mass transfer is highly sensitive to hydrodynamics, small changes in stirring, foaming, surface renewal, and available interfacial area can significantly change the volumetric coefficients $k_L a_{\mathrm{NH_3}}$ and

https://doi.org/10.1021/acs.iecr.6c01013
Ind. Eng. Chem. Res. 2026, 65, 15071−15088

$k_L a_{CO_2}$ from run to run. Finally, Henry constants H_{NH_3} and, H_{CO_2} are temperature dependent and, in practice, behave as effective solubility parameters that can vary with liquid composition TAN, DIC and thus contribute additional uncertainty. We consider parameter uncertainty in this process

$$\boldsymbol{\theta}(\omega) = [k_0(\xi),\ E_a(\xi),\ K_M(\xi),\ K_S(\xi),\ C_E(\xi),\ k_L a_{NH_3}(\xi),\ k_L a_{CO_2}(\xi),\ H_{NH_3}(\xi),\ H_{CO_2}(\xi)]^{\tau}$$

where ξ denotes a basic random vector that parametrizes the uncertainty. The parameters (k_0, E_a, K_M, K_S) characterize the effective urease kinetics in eqs 17−27. In practice, they can vary with enzyme batch-to-batch activity, mild deactivation, and solution conditions such as pH and ionic strength. The factor C_E collects the effective urease loading and activity. The mass transfer coefficients $k_L a_{NH_3}$ and $k_L a_{CO_2}$ depend on mixing intensity and interfacial area, and can therefore vary from run to run. Finally, the Henry constants H_{NH_3} and H_{CO_2} are treated as effective solubility parameters and may vary with temperature and liquid composition. If needed, uncertain initial conditions $(UREA_0, TAN_0, DIC_0)$ can be appended to $\boldsymbol{\theta}(\omega)$.

Under parametric uncertainty, the urea hydrolysis rate becomes a random process because it depends on $\theta(\xi)$ and on the pH computed from the uncertain states via the algebraic charge balance closure. Specifically, using the pH dependent urease kinetics of,[7] we write

$$r_e(t, \xi) = r_e(T(t), \mathrm{pH}(t, \xi), \mathrm{UREA}(t, \xi), \mathrm{TAN}(t, \xi); \theta(\xi))$$

where $\mathrm{pH}(t, \xi) = -\log_{10}(H(t, \xi))$ and $H(t, \xi) = [H^+](t, \xi)$ is obtained by solving the electroneutrality condition together with the speciation relations in eqs 17−27.

Uncertainty in gas−liquid mass transfer enters through the coefficients $k_L a_i(\xi)$ and the Henry constants $H_i(\xi)$ that appear in the transfer relations 21 and 22

$$r_{NH_3,tr}(t, \xi) = k_L a_{NH_3}(\xi)([NH_3](t, \xi) - H_{NH_3}(\xi)P_{NH_3}(t, \xi))$$

$$r_{CO_2,tr}(t, \xi) = k_L a_{CO_2}(\xi)([CO_2^*](t, \xi) - H_{CO_2}(\xi)P_{CO_2}(t, \xi))$$

where $[NH_3](t, \xi)$ and $[CO_2^*](t, \xi)$ are obtained from the speciation model, and $P_i(t, \xi)$ follows from the ideal gas relation in eqs 17−27. These uncertain transfer fluxes modify the evolution of TAN and DIC and thereby affect the computed pH, which in turn feeds back into the urease rate.

2.6.1. Polynomial Chaos Expansion (PCE). Section 2.6 models parametric variability through a random parameter vector $\boldsymbol{\theta}(\boldsymbol{\xi})$. Let $(\Omega, \mathcal{F}, \mathbb{P})$ be a probability space and let $\boldsymbol{\theta}(\omega)$: $\Omega \to \mathbb{R}^b$ be a b-dimensional, real, second-order random vector. We assume that $\boldsymbol{\theta}$ can be parametrized by n independent standard random variables $\boldsymbol{\xi} = (\xi_1, \xi_2, \ldots, \xi_n)$. Under this parametrization, $\boldsymbol{\theta}$ admits a polynomial chaos expansion (PCE)[17]

$$\boldsymbol{\theta}(\boldsymbol{\xi}) = \sum_{i=0}^{\infty} \hat{\boldsymbol{\theta}}_i \psi_i(\boldsymbol{\xi}) \tag{28}$$

where $\{\psi_i(\boldsymbol{\xi})\}$ is an orthonormal polynomial basis in $\mathcal{L}_2(\Omega, \mathcal{F}, \mathbb{P})$ and the coefficient vectors $\{\hat{\boldsymbol{\theta}}_i\} \subset \mathbb{R}^b$ are deterministic.

In practice, we truncate 28 to n_p terms. If we include all polynomials up to total degree P, then $n_p = \binom{n+P}{P}$. Cameron and Martin[18] proved $\mathcal{L}_2$ convergence of the truncated expansions to $\boldsymbol{\theta}(\omega)$, without a general statement on convergence rates. Historically, Wiener's construction focused on Gaussian random processes and used Hermite polynomials, which is why early work often uses the term "Hermite chaos" instead of PCE.[17] Xiu and Karniadakis[19] generalized Hermite chaos by showing that exponential rate of convergence occurs for analytic $\boldsymbol{\theta}$ on increasing P using a polynomial basis whose weighting function is identical to the PDF of the random variables which constitute $\boldsymbol{\xi}$. Using this idea, they formulated the optimal basis for some common random distributions as shown in Table 2,

Table 2. Optimal Basis from the Wiener−Askey Scheme Corresponding to Common Random Distributions

random distribution	optimal basis	support
Gaussian	Hermite	$(-\infty, \infty)$
γ	Laguerre	$(0, \infty)$
β	Jacobi	$(0, 1)$
uniform	Legendre	$(-1, 1)$

and the idea is referred to as *generalized polynomial chaos* (gPC). Owing to this support for a variety of common random distributions, PCE has been applied for probabilistic uncertainty analysis across many disciplines including solid mechanics,[20] fluid mechanics,[21,22] power systems,[23,24] and aerodynamic design optimization.[25] PCE can also be considered for data-driven control.[26] In this formulation, one may distinguish between intrusive and nonintrusive polynomial chaos approaches. In this work, we adopt a nonintrusive strategy also known as stochastic collocation.[27,28] Each model evaluation integrates the ODE balances and, at each time instant, solves the algebraic electroneutrality condition to obtain $H = [H^+]$ and thus pH.

Let $\xi \in \mathbb{R}^d$ be a basic random vector with independent components. The stochastic dimension d equals the number of uncertain quantities included in θ and increases if uncertain initial conditions are appended. In the numerical studies below, we use a reduced stochastic representation with $d = 3$ by retaining the three most influential parameters identified by the local OAT sensitivity screening in Figure 4 and fixing the remaining entries of $\boldsymbol{\theta}(\xi)$ at their nominal values. This reduction is used only for the reported operating regime and controller simulations; it is not intended as a global sensitivity result. Since most parameters are strictly positive, we parametrize uncertainty via a log-normal map

$$\theta_i(\xi) = \bar{\theta}_i \exp(\sigma_i \xi_i), \quad \xi_i \sim \mathcal{N}(0, 1) \tag{29}$$

where $\bar{\theta}_i$ is the nominal value and σ_i sets the coefficient of variation. If we prefer a bounded uncertainty description, we instead use

$$\theta_i(\xi) = \bar{\theta}_i(1 + \delta_i \xi_i), \quad \xi_i \sim \mathcal{U}[-1, 1] \tag{30}$$

with relative bounds $\delta_i \in (0, 1)$. Together, 29 and 30 make clear where uncertainty enters the model. In particular, the kinetic parameters $(k_0, E_a, K_M, K_S, C_E)$ and the transport and

https://doi.org/10.1021/acs.iecr.6c01013
Ind. Eng. Chem. Res. 2026, 65, 15071−15088

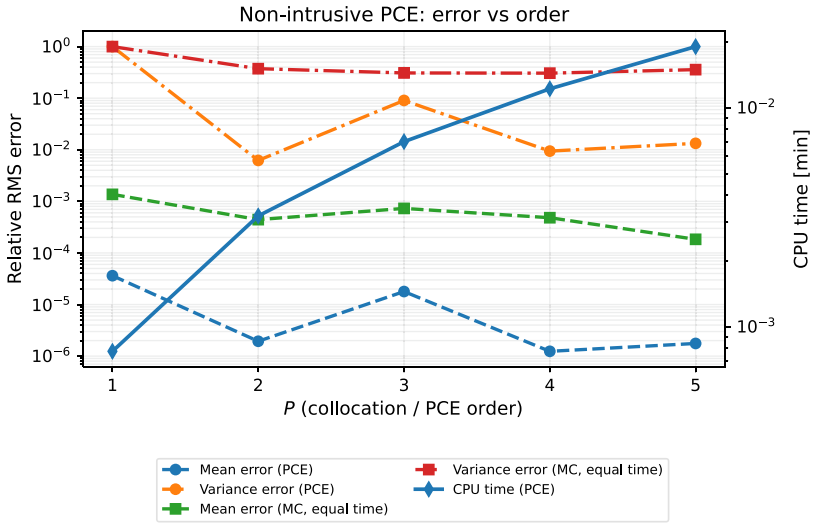

Figure 3. Accuracy cost tradeoff for nonintrusive uncertainty propagation of pH using tensor Gauss-Hermite collocation (gPC) of order P with $N_q = P^d$ nodes $d = 3$ uncertain parameters. Shown are relative RMS errors of the predicted mean and variance, computed with respect to a high-order collocation reference (order P_{ref}), together with the measured CPU time (right axis). Monte-Carlo (MC) errors are computed under an equal CPU time budget for each P by selecting the MC sample size to match the runtime of the collocation calculation.

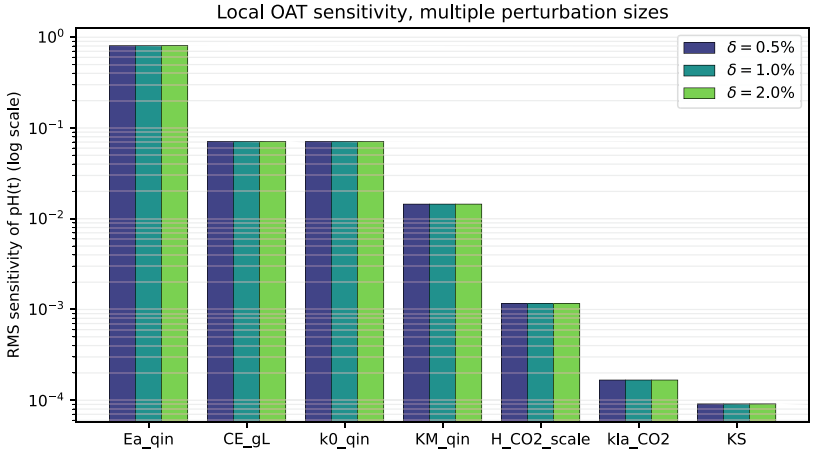

Figure 4. Local OAT sensitivity screening of pH(t), repeated at three relative perturbation sizes $\delta \in \{0.5, 1, 2\%\}$. The RMS sensitivity scores are essentially identical across δ values, confirming that the ranking is not an artifact of the perturbation step size. The three dominant parameters (E_a, k_0, C_E) are 2−4 orders of magnitude more influential than the remaining ones, which justifies reducing the stochastic dimension to $d = 3$ for the SMPC design.

thermodynamic parameters (k_La_i, H_i) are treated as random variables and evaluated as realizations $\boldsymbol{\theta}(\boldsymbol{\xi})$ in each model run. We choose an orthonormal polynomial basis $\{\Psi_k(\boldsymbol{\xi})\}_{k=0}^{N_b}$ with respect to the distribution of $\boldsymbol{\xi}$, so that

$$\mathbb{E}[\Psi_i(\xi)\Psi_j(\xi)] = \delta_{ij} \tag{31}$$

For Gaussian ξ in 29, Ψ_k are multivariate Hermite polynomials, for uniform ξ in 30, Ψ_k are multivariate Legendre polynomials.

Let $x(t, \xi)$ denote the uncertain state trajectory of 16. The quantities of interest in this work are the controlled pH and the reaction rate

$$\mathrm{pH}(t, \xi) = -\log_{10}(H(t, \xi)),\ r_e(t, \xi) \text{given by eqs. (17)} - (27) \tag{32}$$

Both pH(t, ξ) and $r_e(t, \xi)$ become uncertain because they depend on the uncertain parameters $\theta(\xi)$ and on the uncertain states through the ODE-DAE coupling eqs 17−27. We approximate these outputs by truncated PCEs

$$\mathrm{pH}(t, \xi) \approx \sum_{k=0}^{N_b} \widehat{\mathrm{pH}}_k(t)\Psi_k(\xi)$$

$$r_e(t, \xi) \approx \sum_{k=0}^{N_b} \hat{r}_{e,k}(t)\Psi_k(\xi)$$

and, if needed, similarly for selected state components UREA(t, ξ).

Let $\{\xi^{(j)}, w^{(j)}\}_{j=1}^{N_q}$ denote quadrature points and weights in $\mathbb{R}^d$ constructed using either tensor product or sparse grid rules. For each node $\xi^{(j)}$, we run the deterministic simulator with parameters $\theta(\xi^{(j)})$ and input $u(t)$ to obtain trajectories $x^{(j)}(t)$. At each time t, $\mathrm{pH}^{(j)}(t)$ is computed by solving the electroneutrality condition, using the speciation relations of eqs 17−27, and $r_e^{(j)}(t)$ is computed from eqs 17−27. The PCE coefficients are then approximated by weighted projection

https://doi.org/10.1021/acs.iecr.6c01013
Ind. Eng. Chem. Res. 2026, 65, 15071−15088

$$\widehat{\mathrm{pH}}_k(t) \approx \sum_{j=1}^{N_q} w^{(j)} \mathrm{pH}^{(j)}(t) \Psi_k(\xi^{(j)})$$

$$\hat{r}_{e,k}(t) \approx \sum_{j=1}^{N_q} w^{(j)} r_e^{(j)}(t) \Psi_k(\xi^{(j)})$$

By the orthonormality property in 31, the first two moments are immediate. In particular

$$\mathbb{E}[\mathrm{pH}(t)] = \widehat{\mathrm{pH}}_0(t), \quad \mathrm{Var}[\mathrm{pH}(t)] = \sum_{k=1}^{N_b} \widehat{\mathrm{pH}}_k^2(t)$$

$$\mathbb{E}[r_e(t)] = \hat{r}_{e,0}(t), \quad \mathrm{Var}[r_e(t)] = \sum_{k=1}^{N_b} \hat{r}_{e,k}^2(t)$$

In the results section, we summarize uncertainty using bands of the form $\mathbb{E}[\mathrm{pH}(t)] \pm 2\sqrt{\mathrm{Var}[\mathrm{pH}(t)]}$, and we report the corresponding bands for $r_e(t)$ and conversion. These envelopes show how parameter variability propagates to pH trajectories and reaction performance.

Before using gPC moments inside SMPC, we assess the accuracy and computational cost of the nonintrusive gPC propagation for the open-loop pH trajectory. We compute the mean and variance of $y(t) = \mathrm{pH}(t)$ using tensor-product Gauss–Hermite collocation of order P nonintrusive, where the number of model evaluations scales as $N_q = P^d$ for d independent uncertain parameters. Errors are quantified relative to a high order collocation reference (order P_{ref}) under identical model and uncertainty settings.

Figure 3 reports the relative RMS errors in the predicted mean and variance versus P, together with the measured CPU time. As expected, increasing P reduces the moment errors while increasing runtime due to the growth in N_q. For comparison, we also evaluate Monte Carlo propagation under the same computational budget. For each collocation order P, we first record the CPU time required by the corresponding collocation-based PCE calculation. We then choose the number of Monte Carlo samples such that the total Monte Carlo runtime is approximately equal to the recorded collocation runtime. This provides a cost-normalized comparison between collocation-based PCE and Monte Carlo sampling. This comparison motivates the choice of $P = 5$ used in the subsequent SMPC simulations as a suitable accuracy cost compromise. Based on this tradeoff, we use $P = 5$ throughout the SMPC results unless stated otherwise.

2.7. Stochastic MPC for CO_2-Driven pH Regulation

The pH regulation problem in buffer-free urea hydrolysis is governed by two coupled mechanisms (i) *alkalization* due to enzymatic urea conversion and (ii) *acidification* through controlled CO_2 addition. Importantly, the relevant time scale for controller design is not the acid–base chemistry which is treated as instantaneous in our model, but the transport pathway by which the manipulated CO_2 in the gas phase affects the aqueous inorganic carbon pool and thereby pH. Urea hydrolysis produces ammonia and carbon dioxide according to 1. Consequently, the TAN increases at twice the molar production rate of DIC. This 2:1 stoichiometry is the primary driver of the rapid pH rise observed in buffer-free systems. Since urease activity is maximal within a narrow pH window near neutrality, uncontrolled pH drift reduces the effective reaction rate and, ultimately, the overall productivity.

We manipulate the gas-phase CO_2 level in the headspace either via the partial pressure P_{CO_2} or, equivalently, via a CO_2 supply rate. gas–liquid exchange is modeled using a standard driving force law as in the companion manuscript.[1] The aqueous speciation and electroneutrality constraint are enforced at each time instant. Thus, the pH is obtained from $[H^+]$ via $\mathrm{pH} = -\log_{10}([H^+])$. In this actuator pathway, CO_2 influences pH through gas–liquid mass transfer followed by fast acid base equilibria. Under the assumed well mixed conditions, the gas–liquid transfer dynamics induce an approximately first order lag in the effect of CO_2 on pH. A useful characteristic time constant is

$$\tau_{\mathrm{GL}} \approx \frac{1}{kLa}$$

Therefore, if τ_{GL} is not small compared to the pH drift time induced by r_e, purely reactive feedback may be insufficient and anticipatory action is required. This motivates a receding horizon formulation, the controller must begin increasing CO_2 before the pH overshoots the optimal window, because transport limited CO_2 absorption cannot instantaneously correct an excursion. The sampling time and prediction horizon must be chosen relative to the dominant pH-response time scale induced by gas–liquid CO_2 transfer and reaction. Longer horizons can improve anticipation of delayed pH changes. However, they also increase the online prediction effort because the reactor model must be propagated over the uncertainty and over all prediction steps.

In the numerical implementation used here, the CO_2 input is parametrized using a move-blocking strategy, so each candidate control move is held constant over the prediction horizon. The online prediction effort therefore scales approximately as $O(N_u N_q N_p)$, where N_u is the number of candidate input moves, N_q is the number of collocation nodes, and N_p is the prediction horizon. We use $N_p = 2$ for the main simulations as a short-horizon receding-horizon implementation and then assess the sensitivity of the closed-loop response to longer horizons, $N_p = 5$ and 10, in Section 3.3.1. The controlled output in this work is the liquid phase pH

$$y(t, \xi) = \mathrm{pH}(t, \xi) = -\log_{10}(H(t, \xi))$$

where $H(t, \xi) = [H^+](t, \xi)$ is obtained from the electroneutrality closure (Section 2.5). The manipulated input is the CO_2 molar supply rate $u(t) = \dot{n}_{CO_2,\mathrm{supply}}(t)$. The goal is to regulate $\mathrm{pH}(t, \xi)$ to a desired reference $\mathrm{pH}_{\mathrm{ref}}(t)$, which is near the urease optimum despite uncertainty in kinetic and mass transfer parameters $\theta(\xi)$ (Section 2.6).

Let $t_k = k\Delta t$ denote the sampling instants and define $x_k(\xi) = x(t_k, \xi)$, $u_k = u(t_k)$, and $y_k(\xi) = \mathrm{pH}(t_k, \xi)$. Over the prediction horizon N_p, the uncertain model induces predictions

$$x_{k+i+1}(\xi) = F(x_{k+i}(\xi), u_{k+i}; \theta(\xi)) \tag{33}$$

$$y_{k+i}(\xi) = h(x_{k+i}(\xi); \theta(\xi)) \tag{34}$$

where $F(\cdot)$ represents numerical integration of the coupled ODE-DAE reactor model in Sections 2.5, and $h(\cdot)$ denotes the algebraic mapping from (x, θ) to pH obtained by solving the electroneutrality condition. Given a candidate input sequence $U_k = \{u_k, \ldots, u_{k+N_p-1}\}$, we compute the predicted pH statistics

https://doi.org/10.1021/acs.iecr.6c01013
Ind. Eng. Chem. Res. 2026, 65, 15071–15088

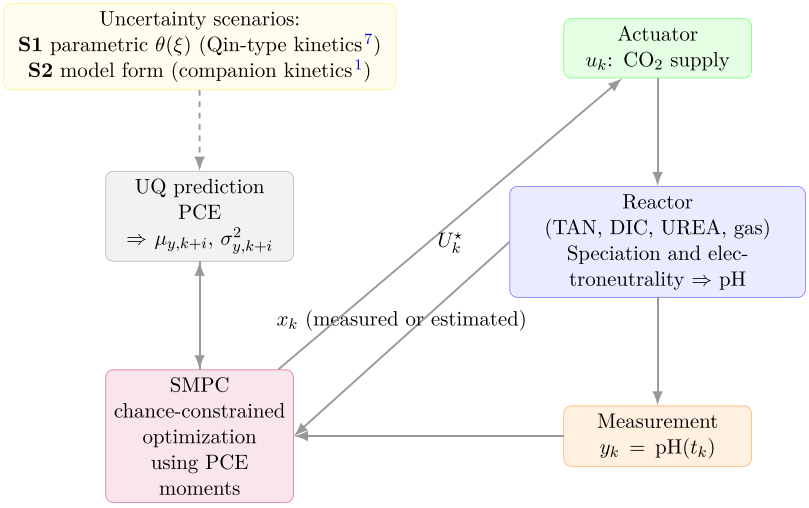

Figure 5. Closed-loop workflow for CO_2-driven pH regulation with uncertainty-aware prediction and SMPC. At each sampling instant t_k, the SMPC is initialized with the current reactor state x_k, assumed to be available either from direct measurement or from a deterministic state observer. The parametric uncertainty description $\theta(\xi)$ is fixed *offline* from prior identification and the sensitivity screening of Section 3.2, the PCE module uses it to compute the predicted moments $\mu_{y,k+i}$ and $\sigma^2_{y,k+i}$ over the horizon. No online parameter estimation is performed. The controlled output is $y_k = \mathrm{pH}(t_k)$. Scenario 1 (S1) corresponds to parametric variability $\theta(\xi)$ within the Qin-type kinetic model used by the SMPC, while Scenario 2 (S2) replaces the plant kinetic law by the companion kinetics[1] to assess closed-loop sensitivity to structural model mismatch.

using the same collocation nodes $\{\xi^{(j)}, w^{(j)}\}_{j=1}^{N_q}$ as in Section 2.6.1. For each node $\xi^{(j)}$ we simulate eqs 33 and 34 forward with parameters $\theta(\xi^{(j)})$ and obtain trajectories $y^{(j)}_{k+i}$. The mean and variance predictions are then approximated by

$$\mu_{y,k+i} = \mathbb{E}[y_{k+i}] \approx \sum_{j=1}^{N_q} w^{(j)} y^{(j)}_{k+i}$$

$$\sigma^2_{y,k+i} = \mathrm{Var}[y_{k+i}] \approx \sum_{j=1}^{N_q} w^{(j)} (y^{(j)}_{k+i} - \mu_{y,k+i})^2$$

We assume that, at each sampling instant t_k, the full reactor state x_k is available to the controller, either through direct measurement of UREA, TAN, and DIC together with the gas-phase inventories, or through a deterministic state observer. The design of such an observer is outside the scope of this work. The parametric uncertainty description $\theta(\xi)$ is fixed *offline*, based on prior identification studies and on the local sensitivity screening of Section 3.2; no online re-estimation of $\theta(\xi)$ is performed during closed-loop operation. At each sampling instant, every collocation node is initialized with the same measured or estimated state x_k, and only the uncertain parameters $\theta(\xi^{(j)})$ vary across nodes. Under these assumptions, we pose the following finite-horizon SMPC problem with hard input bounds and joint chance constraints

$$\min_{U_k} \sum_{i=0}^{N_p-1} \left(w_{\mathrm{pH}} (\mu_{y,k+i} - \mathrm{pH}_{\mathrm{ref},k+i})^2 + w_\sigma \sigma^2_{y,k+i} + w_u u^2_{k+i} + w_{\Delta u} (u_{k+i} - u_{k+i-1})^2 \right) \tag{35}$$

$$\text{s. t. } x_{k+i+1}(\xi^{(j)}) = F(x_{k+i}(\xi^{(j)}), u_{k+i}; \theta(\xi^{(j)})), \quad j = 1, \ldots, N_q,\ i = 0, \ldots, N_p - 1 \tag{36}$$

$$0 \le u_{k+i} \le u_{\max}, \quad i = 0, \ldots, N_p - 1 \tag{37}$$

$$\mathbb{P}(y_{\min} \le y_{k+i}(\xi) \le y_{\max}) \ge 1 - \varepsilon, \quad i = 0, \ldots, N_p - 1 \tag{38}$$

The objective 35 is designed to track the desired pH while accounting for uncertainty and actuation effort. It minimizes the mean pH tracking error, optional variance reduction, and regularizes the control action through CO_2 usage and rapid input changes. To enforce the chance constraints 38 in a tractable manner, we employ a moment-based approximation as a surrogate for the original probabilistic constraints.[29,30] Because pH is computed from a nonlinear electroneutrality equation, the predicted pH distribution is not guaranteed to be exactly Gaussian. Nevertheless, the PCE-based collocation prediction provides the mean and variance of the pH output, namely $\mu_{y,k+i}$ and $\sigma^2_{y,k+i}$. We denote the corresponding standard deviation by $\sigma_{y,k+i} = \sqrt{\sigma^2_{y,k+i}}$. Under a Gaussian approximation of the scalar predicted pH output, the two-sided chance constraint in 38 is enforced through

$$y_{\min} \le \mu_{y,k+i} - \kappa^G_\varepsilon \sigma_{y,k+i}, \quad \mu_{y,k+i} + \kappa^G_\varepsilon \sigma_{y,k+i} \le y_{\max} \tag{39}$$

where $\kappa^G_\varepsilon = \Phi^{-1}(1 - \varepsilon/2)$ and $\Phi^{-1}(\cdot)$ is the standard normal quantile.[30] This is a tractable Gaussian moment approximation of the original probabilistic constraint, not an exact reformulation for arbitrary pH distributions.

Alternatively, the same moments computed from the PCE-based collocation predictions can be used in a distribution-free tightening. By Chebyshev's inequality

$$\mathbb{P}(|y_{k+i} - \mu_{y,k+i}| \ge \kappa^C_\varepsilon \sigma_{y,k+i}) \le \frac{1}{(\kappa^C_\varepsilon)^2} \tag{40}$$

Thus, choosing $\kappa^C_\varepsilon = 1/\sqrt{\varepsilon}$ and enforcing

$$y_{\min} \le \mu_{y,k+i} - \kappa^C_\varepsilon \sigma_{y,k+i}, \quad \mu_{y,k+i} + \kappa^C_\varepsilon \sigma_{y,k+i} \le y_{\max} \tag{41}$$

provides a distribution-free sufficient condition for 38, provided the predicted pH has finite variance. Distributionally robust and Chebyshev-Cantelli-type backoff constructions are standard in chance-constrained optimization and stochastic NMPC.[23,31]

https://doi.org/10.1021/acs.iecr.6c01013
Ind. Eng. Chem. Res. 2026, 65, 15071−15088

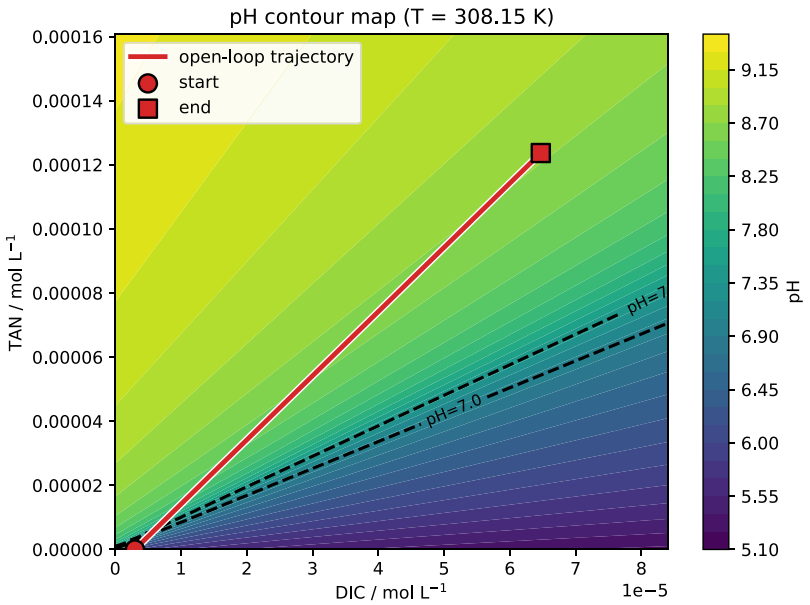

Figure 6. Equilibrium pH contour map in TAN−DIC space at T = 308.15 K. The dashed black contours indicate the pH safety bounds pH = 7.0 and 7.4. The solid orange-red curve overlaid on the map is the open-loop trajectory of the reactor in composition space, with the circle marking the initial state and the square marking the final state; it illustrates how the evolving TAN and DIC composition drives the pH excursion observed under buffer-free operation.

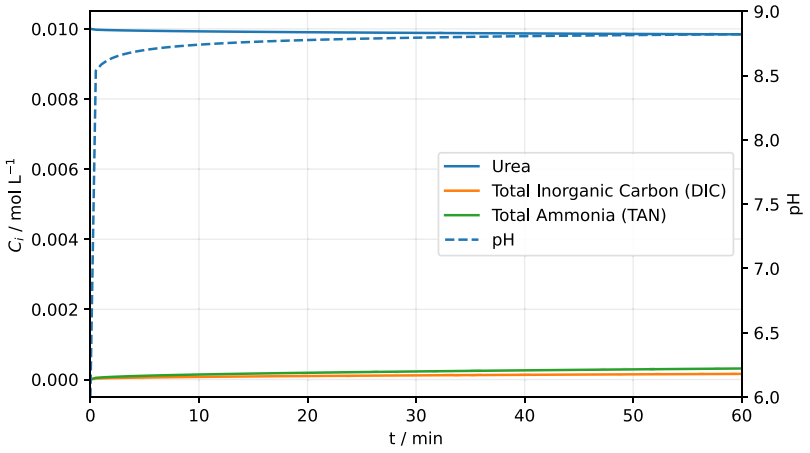

Figure 7. Open-loop time profiles of UREA, TAN, DIC, and pH. The pH rapidly drifts to an alkaline plateau under buffer-free operation, motivating feedback control via CO_2 dosing.

For ε = 0.05, the Gaussian factor is $\kappa_\varepsilon^G \approx 1.96$, whereas the Chebyshev factor is $\kappa_\varepsilon^C \approx 4.47$.

The SMPC is implemented as follows, at time t_k, the current state is measured or estimated, the optimization problem eqs 35−38 is solved using the Gaussian moment tightening 39, the first control input u_k* is applied, and the horizon is shifted to t_{k+1}. The Chebyshev inequality in 41 provides a distribution-free alternative based on the same predicted moments computed from the PCE collocation model, but it is not used for the main closed-loop simulations because of its additional conservatism. This yields closed-loop regulation of pH via CO_2 dosing despite parametric variability in kinetics and gas−liquid transfer.

3. NUMERICAL RESULTS

This section evaluates the proposed uncertainty-aware SMPC framework in simulation. All closed-loop results in this section are simulation-based. The purpose of the numerical study is to evaluate the proposed uncertainty-aware SMPC formulation under the control-oriented reactor model described in Sections 2.5−2.7. No physical closed-loop reactor experiment is performed in the present manuscript. Therefore, the results should be interpreted as a computational assessment of controller behavior under parametric uncertainty and selected model-form mismatch, rather than as experimental validation of closed-loop performance. We first examine the uncontrolled open-loop behavior to highlight the intrinsic pH drift that arises in buffer-free operation and motivates the need for active CO_2 dosing. We then quantify the impact of parametric uncertainty using PCE and finally demonstrate closed-loop performance under the proposed stochastic MPC strategy.

This section demonstrates (i) why buffer-free urea hydrolysis exhibits large pH excursions under open-loop operation, (ii) how the TAN-DIC composition explains these excursions, and (iii) how the proposed PCE-collocation SMPC uses CO_2 dosing to regulate pH while explicitly accounting for parametric uncertainty.

https://doi.org/10.1021/acs.iecr.6c01013
Ind. Eng. Chem. Res. 2026, 65, 15071−15088

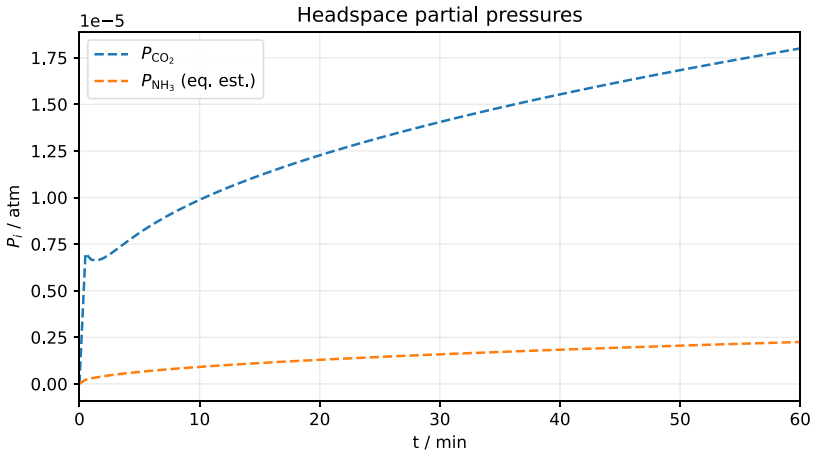

Figure 8. Open-loop headspace partial pressures predicted by the gas−liquid mass transfer model. CO_2 increases rapidly and then gradually, while NH_3 remains lower, confirming the coupling between gas dosing and liquid phase speciation relevant for pH regulation.

3.1. Open-Loop Behavior

This open-loop analysis motivates stochastic MPC by illustrating how uncertainty in kinetics and gas−liquid transfer can shift the TAN and DIC trajectory and hence the pH drift. A key advantage of the mechanistic formulation is that it provides an interpretable link between the conserved totals TAN, DIC and the resulting pH. Figure 6 visualizes the equilibrium pH as a function of TAN-DIC at the operating temperature. As discussed in the companion modeling and experimental study,[1] this TAN-DIC representation explains the direction and magnitude of pH drift in buffer-free urea hydrolysis, increasing TAN at fixed DIC drives pH upward, whereas increasing DIC at fixed TAN drives pH downward due to increased carbonic acid buffering capacity. The plotted open-loop trajectory indicates how the reaction moves the system through this composition space, so the pH excursion is an expected thermodynamic consequence of evolving TAN and DIC.

Figure 7 shows the corresponding open-loop reactor evolution in time in terms of total species (UREA, TAN, and DIC) together with the resulting pH trajectory. Even though the totals evolve smoothly, the pH exhibits a rapid drift toward an alkaline regime and then remains near a high plateau. This highlights why buffer-free operation is challenging, comparatively small changes in TAN and DIC composition can translate into large changes in pH, pushing the reactor away from the desired operating window.

To connect the liquid phase composition with what is observed in the gas phase, Figure 8 reports the predicted headspace partial pressures. The CO_2 partial pressure rises rapidly and then increases more gradually, while NH_3 remains comparatively lower over the same horizon. This confirms that gas−liquid coupling is active and that manipulating CO_2 dosing is a physically meaningful lever for shifting the inorganic carbon system and therefore pH.

This TAN and DIC view also clarifies the control task: to keep pH near neutral while TAN accumulates, the system must be steered toward higher effective DIC relative to TAN, which is precisely what CO_2 dosing accomplishes through dissolution and subsequent speciation. This interpretation provides the main chemical-engineering insight of our study. The controller is not simply correcting pH as an abstract output; it is actively reshaping the TAN−DIC composition pathway followed by the reacting mixture. In buffer-free urea hydrolysis, TAN formation moves the system toward alkaline conditions, while CO_2 dosing increases the DIC inventory and shifts carbonate speciation so that the pH trajectory remains near the urease-optimal range. Thus, the SMPC action can be interpreted chemically as controlled management of the TAN-DIC ratio under reaction and gas−liquid-transfer uncertainty. This viewpoint connects the control law to process operation and helps identify which physical mechanisms, enzyme activity, CO_2 transfer, and carbonate buffering capacity, should be calibrated or monitored in future experiments.

3.2. Sensitivity analysis of the pH dynamics

The uncertainty bands in the previous subsection show that parameter variability can noticeably widen the pH trajectory. In a buffer-free system, it is just as important to identify *which* parameters actually drive that spread near the nominal operating point. We care about this for three practical reasons. First, pH is obtained by solving a nonlinear charge-balance equation, so small parameter changes can translate into large pH shifts. Second, the manipulated input affects pH mainly through the CO_2 transfer pathway, so uncertainties in transfer and solubility can dominate closed-loop behavior even if kinetic parameters are also uncertain. Third, a sensitivity ranking tells us what to prioritize for calibration or online estimation, and what can be fixed to reduce the stochastic dimension in the SMPC design. To get a simple and easy-to-interpret ranking, we perform a *local one-at-a-time (OAT) sensitivity screening* around the nominal parameter set. We simulate the nominal model over a time horizon T (here $T = 60$ min) under a fixed input used only for screening, for example $u(t) \equiv 0$. Let $\theta = [\theta_1, \ldots, \theta_m]$ denote the selected parameters for example, C_E, k_0, E_a, K_M, K_S, $k_L a_{CO_2}$. The output of interest is the pH trajectory $y(t;\theta) = \mathrm{pH}(t;\theta)$ obtained from the coupled ODE-DAE model.

For each parameter θ_i, we apply multiplicative perturbations with a relative step size δ

$$\theta_i^+ = \theta_i(1+\delta), \qquad \theta_i^- = \theta_i(1-\delta) \tag{42}$$

while keeping all other parameters fixed at their nominal values. We simulate the model for θ_i^+ and θ_i^- and obtain $y_i^+(t)$ and $y_i^-(t)$ on the same time grid. We then compute a local sensitivity signal via a central difference

$$s_i(t) := \frac{y_i^+(t) - y_i^-(t)}{2\delta}$$

https://doi.org/10.1021/acs.iecr.6c01013
Ind. Eng. Chem. Res. 2026, 65, 15071−15088

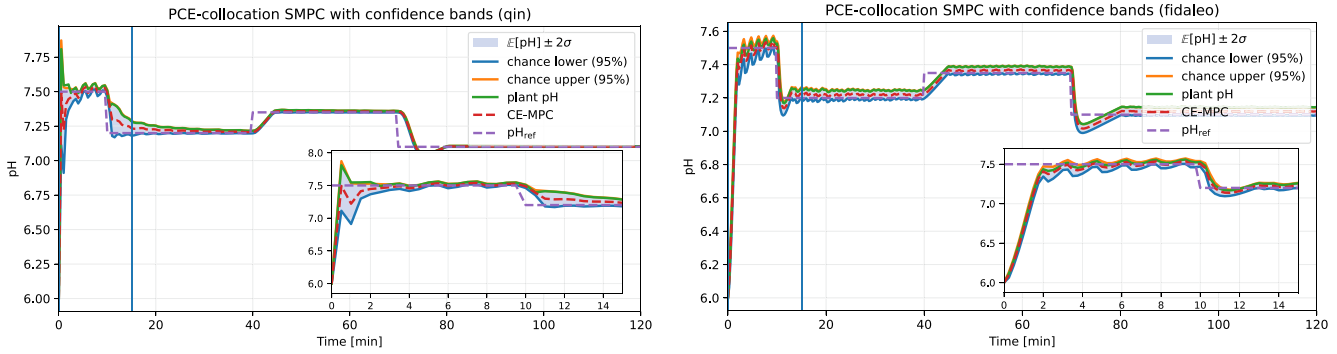

(a) Closed-loop pH regulation with the Qin-type model.

(b) Closed-loop pH regulation with the Fidaleo-type model.

Figure 9. Closed-loop pH regulation using PCE-collocation SMPC. (a) Parametric-uncertainty case: the SMPC prediction model and the simulated plant both use the Qin-type kinetic law, while selected kinetic and transfer parameters are uncertain. (b) Structural-mismatch case: the SMPC prediction model uses the Qin-type kinetic law, while the simulated plant uses the companion kinetic law. The solid curve shows the plant pH, the dashed prediction curve shows the one-step-ahead predicted mean pH used by the SMPC, and the reference trajectory is labeled as pH_{ref}. Uncertainty is summarized by the band $\mathbb{E}[pH] \pm 2\sigma$ and by the empirical 95% chance bounds. Panel (b) should be interpreted as a simulation-based stress test of kinetic model-form mismatch rather than as a formal robustness guarantee.

Because the perturbation is multiplicative, $s_i(t)$ approximates $\partial y(t;\theta)/\partial \ln(\theta_i)$. In other words, it measures how much the pH changes when θ_i is changed by a small *percentage*. To rank parameters, we compress each sensitivity signal to a single number using its root-mean-square (RMS) value over the horizon

$$\text{Score}_i := \sqrt{\frac{1}{N}\sum_{k=1}^{N} s_i^2(t_k)} \tag{43}$$

where $\{t_k\}_{k=1}^{N}$ is the simulation time grid. A larger Score_i means that small relative changes in θ_i produce larger deviations in the pH trajectory near the nominal operating point. The nonlinear algebraic pH computation can make perturbed simulations numerically fragile. If a perturbed run produces NaN/Inf values or nonphysical pH, we discard that run and do not use it to form the finite difference. If perturbations of a particular parameter repeatedly lead to invalid simulations, we flag that parameter as *critical* for reliable prediction and control. In practice, this points to the need for tighter bounds, better calibration, or additional measurements for that mechanism. This screening often shows why only a subset of parameters matters locally. Near the nominal trajectory, pH is mainly set by the balance between TAN kinetics and CO_2 absorption and carbonate speciation of transfer and solubility. Parameters that strongly influence these pathways tend to rank highest, while parameters that enter weakly in the operating regime visited here yield small scores. We use the resulting ranking to prioritize calibration or estimation efforts and reduce the uncertainty dimension in subsequent UQ and SMPC studies by fixing low-impact parameters to their nominal values. The perturbation sizes $\delta \in \{0.5, 1, 2\%\}$ are used to check whether the ranking depends on the finite-difference step size. If the ranking changes substantially when δ is changed, then the screening result may be a numerical artifact of the perturbation size. In contrast, if the same dominant parameters are obtained for all three values of δ, the ranking is more reliable as a local sensitivity result. In the present case, the ranking is essentially unchanged across these perturbation sizes, indicating that the selection of E_a, k_0, and C_E is not caused by an arbitrary choice of δ.

We emphasize that this reduction is local. The ranking is tied to the nominal trajectory, perturbation range, and screening input used here, and it may change under different operating conditions or closed-loop input profiles. Thus, the reduced $d = 3$ uncertainty representation should be interpreted as a practical dimension reduction choice for the numerical SMPC case study, not as a global claim that the remaining parameters are always negligible. For operation in a different regime, the screening should be repeated using representative closed-loop trajectories, or replaced by a global sensitivity analysis such as Sobol or variance-based screening.

3.3. Uncertainty-Aware Control via SMPC

To test the proposed control scheme, we consider two scenarios:

- Scenario 1 (parametric model uncertainty): We design and evaluate closed-loop pH regulation assuming a fixed model structure based on Qin-type kinetics, with uncertainty represented through kinetic and transport parameters. At each sampling time, we propagate the parameter uncertainty over the prediction horizon using a nonintrusive PCE collocation strategy, yielding time-resolved predictions of the pH distribution. These predictions are embedded in a SMPC formulation that selects the CO_2 dosing rate to track a desired pH reference while maintaining probability satisfaction of the pH safety window.

- Scenario 2 (structural model mismatch): The plant kinetic model differs from the Qin-type kinetics used inside the SMPC prediction model. Specifically, the controller is designed using the Qin-type kinetic law, while the simulated plant uses the companion kinetic law.[1] This setting is not captured by the parametric uncertainty distribution used in the PCE model, because it represents a change in the reaction-rate expression rather than a perturbation of parameters within a fixed model form. Therefore, Scenario 2 is used as an out-of-model stress test of closed-loop sensitivity to kinetic model-form errors. It should not be interpreted as a formal robustness guarantee.

https://doi.org/10.1021/acs.iecr.6c01013
Ind. Eng. Chem. Res. 2026, 65, 15071−15088

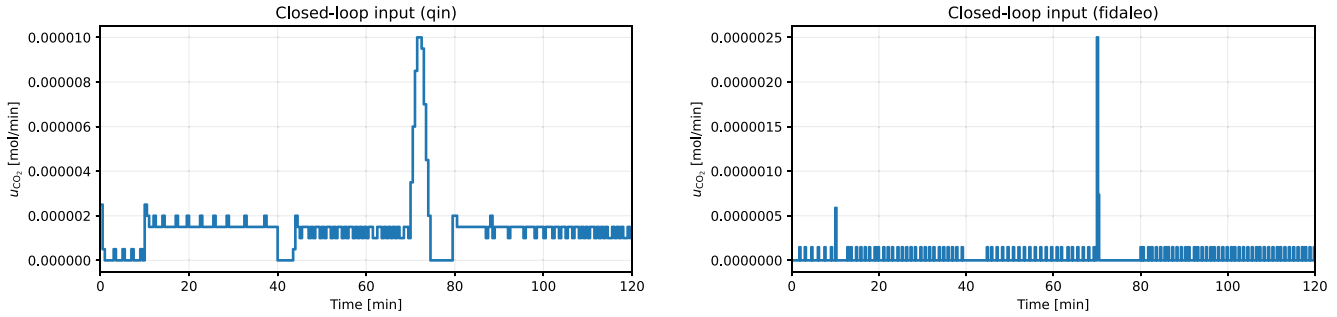

(a) Closed-loop CO_2 dosing with the Qin-type model.

(b) Closed-loop CO_2 dosing with the Fidaleo-type model.

Figure 10. Closed-loop CO_2 dosing profiles generated by the PCE-collocation SMPC. (a) Input profile for the Qin-type kinetic model. (b) Input profile for the structural-mismatch case in which the simulated plant uses the companion kinetic law. In both panels, the input remains within the imposed bound and changes in a piecewise-constant manner due to the receding-horizon implementation.

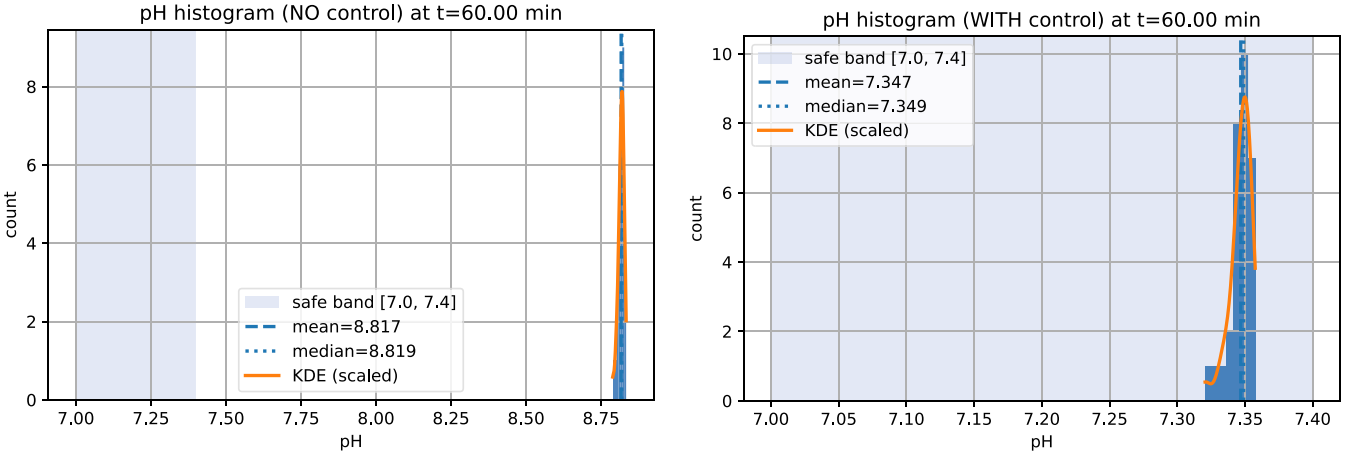

Figure 11. pH distribution at $t = 60$ min under parametric uncertainty. Left: under open-loop operation, the no-control distribution lies far above the safe band [7.0, 7.4] mean ≈ 8.817. Right: closed-loop distribution under SMPC is shifted into the safe band (mean ≈ 7.347), demonstrating distributional risk-aware regulation rather than only nominal tracking.

Figure 5 summarizes the overall closed-loop workflow together with the two uncertainty scenarios that we consider in this paper: Scenario 1 (parametric uncertainty within the Qin-type kinetic model) and Scenario 2 (structural model mismatch obtained by replacing the plant kinetics with the companion law).

Figure 9 shows the resulting closed-loop pH response together with uncertainty summaries. The solid curve is the plant pH, while the dashed prediction summarizes the one-step-ahead expected pH used by the controller. The shaded bands visualize uncertainty in two complementary ways: an empirical 95% interval and a mean $\pm 2\sigma$ band. The key point is not only that the mean tracks the reference, but that the predicted dispersion remains small enough to support probabilistic safety. In other words, the controller is not tuned only for nominal tracking; it is explicitly shaped by uncertainty forecasts.

The CO_2 dosing profile that produces this behavior is shown in Figure 10. The input remains bounded and exhibits piecewise constant behavior consistent with receding-horizon optimization. Short transients or spikes occur when the controller must quickly correct the predicted risk of leaving the desired pH region, for example after a reference change or a shift in the predicted dynamics. After these corrective actions, the input returns to a lower maintenance level, indicating that regulation does not require persistently aggressive dosing.

At each sampling time t_k, the prediction model is initialized with the current reactor state x_k, which is assumed to be available through direct measurement or a deterministic observer, no online parameter estimation is performed. Each collocation node is initialized with the same x_k, and only the uncertain parameters $\theta(\xi^{(j)})$ vary across nodes. The controlled output is $y_k = \mathrm{pH}(t_k) = h(x_k)$, computed from TAN and DIC via the electroneutrality closure. Finally, we compare the pH distributions at a representative time snapshot. Figure 11a shows the pH histogram at $t = 60$ min without control, the distribution is concentrated far above the safe band [7.0, 7.4], with mean ≈ 8.817 and median ≈ 8.819, implying near certain violation of the desired operating window. In contrast, Figure 11b shows the same snapshot under closed-loop control, the distribution is shifted into the safe band, with mean ≈ 7.347 and median ≈ 7.349. This paired comparison highlights the central benefit of the proposed approach: the SMPC does not merely propagate uncertainty in its predictions, it actively manages it, so that the entire pH distribution and not only a single nominal trajectory is steered into the desired operating window.

Figure 9a,b compare two different uncertainty settings. In Figure 9a, the SMPC prediction model and the simulated plant

https://doi.org/10.1021/acs.iecr.6c01013
Ind. Eng. Chem. Res. 2026, 65, 15071−15088

Table 3. Simulation, Uncertainty Propagation, and SMPC Settings Used for All Numerical Results

item	value
sampling time	Δt = 0.5 min (30 s)
evaluation horizon	T = 120 min
prediction horizon	main simulations: N_p = 2 steps (T_p = 1 min); diagnostic horizons: $N_p \in \{2, 5, 10\}$
input bounds	$0 \le u \le u_{max}$, $u_{max} = 1 \times 10^{-5}$ mol/min
PCE order	P = 5
collocation rule	Gauss−Hermite
number of nodes	N_q = 125
objective weights	$w_{pH} = 500$, $w_\sigma = 0$, $w_u = 10^5$, $w_{\Delta u} = 2 \times 10^6$
chance constraint	confidence = 0.95 (ϵ = 0.05). Gaussian tightening: $\kappa_\varepsilon^G = \Phi^{-1}(0.975) \approx 1.96$. Chebyshev tightening: $\kappa_\varepsilon^C = 1/\sqrt{0.05} \approx 4.47$

both use the Qin-type kinetic law. The uncertainty is therefore parametric: the kinetic and transfer parameters vary within the fixed model structure used by the controller. This case is consistent with the PCE uncertainty description used inside the SMPC, and the predicted uncertainty bands remain aligned with the closed-loop response after the initial transient.

Figure 9b considers a different situation. The SMPC prediction model still uses the Qin-type kinetic law, whereas the simulated plant uses the companion kinetic law. Thus, the discrepancy is structural rather than purely parametric: the reaction-rate expression itself changes. The resulting response shows that kinetic model-form errors can alter the pH drift and reduce the accuracy of the one-step-ahead prediction. Consequently, Figure 9b should be interpreted as an empirical out-of-model stress test, not as a formal robustness guarantee.

A formal robustness guarantee for this case would require an explicit model-discrepancy description, for example

$$x_{k+1}^{plant} = F_{Qin}(x_k, u_k; \theta) + d_k, \quad \|d_k\| \le \overline{d} \tag{44}$$

or an equivalent bound on the pH prediction error

$$|y_{k+i}^{plant} - y_{k+i}^{Qin}| \le \overline{\delta}_{pH} \tag{45}$$

Such a bound could be incorporated through pH constraints, for example

$$y_{min} + \overline{\delta}_{pH} \le \mu_{y,k+i} - \kappa_\varepsilon \sigma_{y,k+i},$$
$$\mu_{y,k+i} + \kappa_\varepsilon \sigma_{y,k+i} \le y_{max} - \overline{\delta}_{pH} \tag{46}$$

This extension is outside the scope of the present study and motivates future work on model discrimination, online model adaptation, and experimental closed-loop validation when the kinetic law is uncertain.

All simulation, uncertainty propagation, and SMPC settings used in this study are summarized in Table 3.

3.3.1. Prediction-Horizon Sensitivity. The main SMPC simulations use N_p = 2, corresponding to a prediction horizon of $T_p = N_p \Delta t$ = 1 min for Δt = 0.5 min. To check whether the closed-loop behavior depends critically on this short horizon, we repeated the Qin-type parametric-uncertainty case using longer horizons, N_p = 5 and 10, while keeping the same sampling time, constraints, uncertainty description, and objective weights.

Figure 12 compares the resulting closed-loop pH responses. The longer horizons produce comparable pH regulation and do not change the qualitative conclusion that CO_2 dosing can keep the pH close to the desired operating window under the considered parametric uncertainty. This indicates that the results reported for N_p = 2 are not an artifact of the short prediction horizon. Therefore, N_p = 2 is used in the main simulations as a short-horizon setting with lower online prediction effort for the present numerical case. This should not be interpreted as a general claim that longer horizons are unnecessary; rather, the horizon-sensitivity test indicates that the selected sampling time and feedback update are sufficient for the considered operating regime.

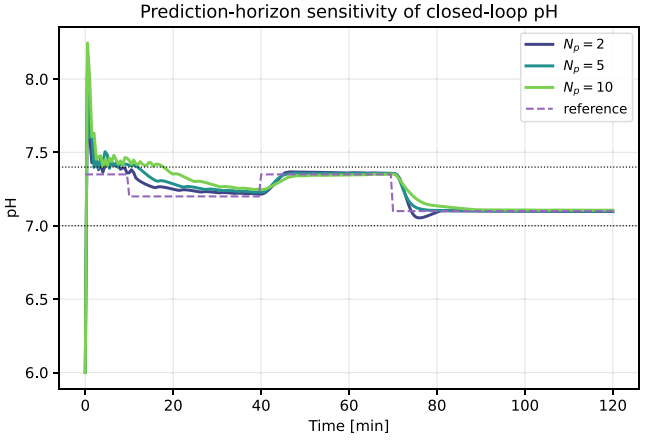

Figure 12. Prediction-horizon sensitivity of the closed-loop pH response for $N_p \in \{2, 5, 10\}$. The same sampling time, constraints, uncertainty description, and objective weights are used in all cases. The comparison shows that the main closed-loop behavior is not an artifact of the short N_p = 2 horizon.

3.3.2. Gaussian Moment Approximation. The Gaussian tightening in 39 is used as a tractable moment-based approximation of the chance constraint. Since pH is computed from a nonlinear electroneutrality calculation, the predicted pH distribution is not guaranteed to be Gaussian. Therefore, we assess the adequacy of this approximation for the present numerical case by evaluating a representative one-step prediction at t = 30 min using the current closed-loop state, the one-step SMPC input, and the same PCE parameter samples used in the controller.

Figure 13 compares the resulting pH samples with a Gaussian distribution having the same mean and variance. The predicted pH distribution is close to Gaussian for this representative prediction step, with mean 7.210, standard deviation 0.007, skewness 0.02, and excess kurtosis 0.12. The empirical probability of satisfying the safety interval 7.0 ≤ pH ≤ 7.4 is 1.000.

Figure 14 shows the corresponding weighted Q−Q diagnostic. The near-linear alignment supports the Gaussian moment approximation for this representative one-step prediction. However, Gaussianity is not claimed as a general property of the nonlinear pH model.

https://doi.org/10.1021/acs.iecr.6c01013
Ind. Eng. Chem. Res. 2026, 65, 15071−15088

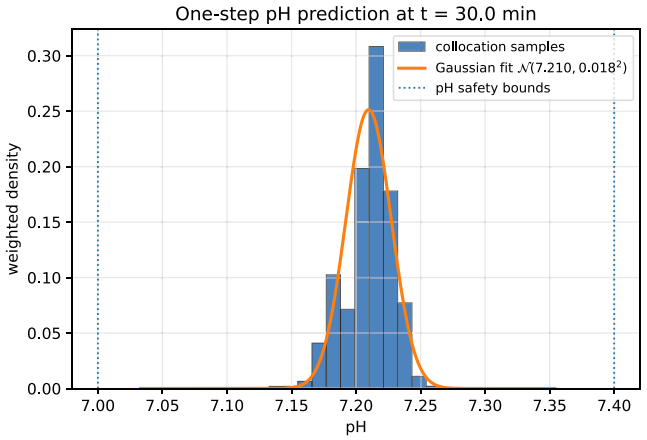

Figure 13. Distribution of the one-step pH prediction at t = 30 min, compared with a Gaussian distribution having the same mean and variance. The vertical dotted lines indicate the pH safety bounds.

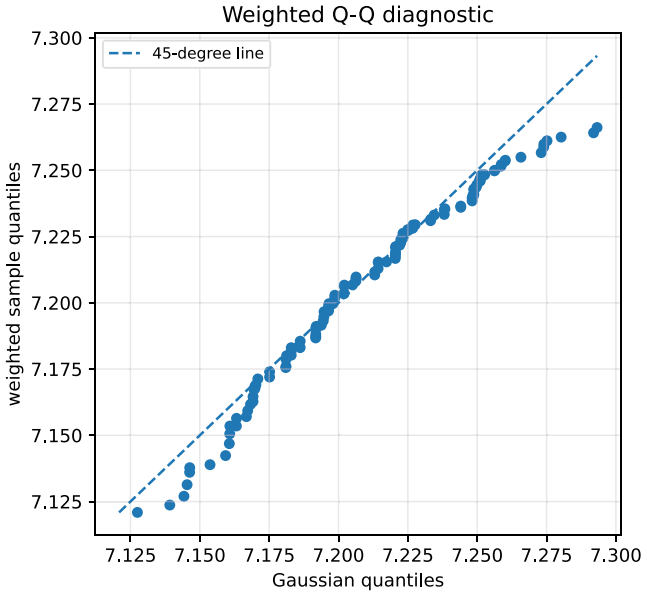

Figure 14. Weighted Q−Q diagnostic for the one-step pH prediction at t = 30 min. The near-linear alignment supports the Gaussian moment approximation for this representative prediction step, while Gaussianity is not claimed as a general property of the nonlinear pH model.

3.3.3. Distribution-Free Chebyshev Approximation.

To show how the moment-based chance constraint can be enforced without a Gaussian approximation, we also state the corresponding distribution-free Chebyshev tightening in 41. The same PCE predictions of the mean $\mu_{y,k+i}$ and variance $\sigma^2_{y,k+i}$ are used, the standard deviation $\sigma_{y,k+i}$ is used in the tightening bounds.

Since $\kappa^C_\varepsilon = 1/\sqrt{\varepsilon}$ is larger than $\kappa^G_\varepsilon = \Phi^{-1}(1 - \varepsilon/2)$, the Chebyshev tightening imposes a wider backoff from the pH safety limits. For $\varepsilon = 0.05$, this gives $\kappa^C_\varepsilon \approx 4.47$, compared with $\kappa^G_\varepsilon \approx 1.96$. Therefore, the distribution-free Chebyshev formulation is more conservative than the Gaussian moment approximation and may require larger CO_2 usage or reduce feasibility margins. Nevertheless, the formulation demonstrates that the PCE-SMPC framework itself does not rely on Gaussianity of the pH distribution: the same predicted mean and variance can be combined with either a Gaussian tightening or a distribution-free Chebyshev tightening.

3.3.4. Comparison with Certainty-Equivalent MPC.

To assess the value of the stochastic formulation, we compare the proposed SMPC with a certainty-equivalent MPC baseline. The certainty-equivalent MPC uses the same sampling time, prediction horizon, input constraints, reference trajectory, and objective weights as the proposed SMPC. The only difference is that all uncertain parameters are fixed at their nominal values inside the prediction model. Thus, CE-MPC is a nominal receding-horizon controller; it is not a worst-case or robust controller. In contrast, the proposed SMPC propagates the modeled parameter uncertainty through the PCE and uses the predicted pH mean and variance in the chance-constraint tightening.

Figure 15 shows that both CE-MPC and SMPC substantially improve pH regulation relative to open-loop operation.

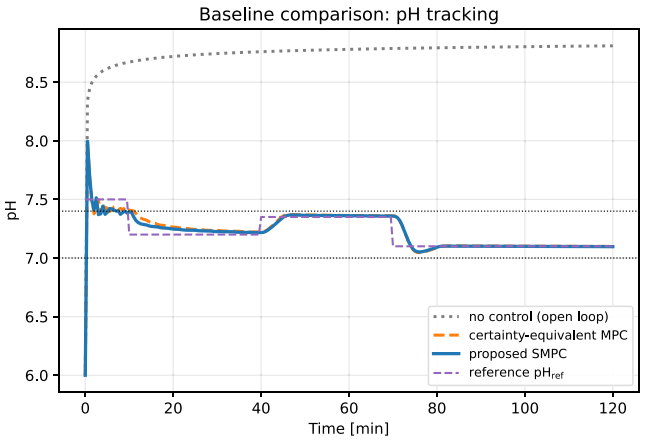

Figure 15. Baseline comparison of pH tracking between open-loop operation, certainty-equivalent MPC, and the proposed SMPC. The certainty-equivalent MPC uses the same objective, constraints, sampling time, and prediction horizon as the proposed SMPC, but fixes all uncertain parameters at their nominal values.

However, this nominal tracking comparison alone does not fully show the value of the stochastic formulation, because CE-MPC can also regulate the nominal pH trajectory. The relevant difference is how the two controllers behave when the actual plant parameters differ from the nominal values. The corresponding CO_2 dosing profiles for the open-loop, CE-MPC, and SMPC cases are shown in Figure 16.

To isolate this effect, we evaluate CE-MPC and SMPC on the same set of uncertain plant realizations. For CE-MPC, the controller predicts using nominal parameter values, but the resulting input is applied to uncertain plant samples. For SMPC, the same uncertainty distribution is propagated through the PCE/collocation prediction model and enters the chance-constraint tightening through the predicted pH mean and variance.

Figure 17 and Table 4 show the tradeoff between nominal tracking and probabilistic safety. CE-MPC gives slightly lower mean tracking errors because it regulates the nominal prediction without an uncertainty margin. However, CE-MPC accumulates larger pH safety violations when applied to uncertain plant realizations, while SMPC reduces these violations through the chance-constraint tightening based on the propagated PCE moments.

Table 4 reports two metric sets: one over the full simulation horizon and one after the startup transient. The full-horizon metrics quantify the total closed-loop behavior from the initial

https://doi.org/10.1021/acs.iecr.6c01013
Ind. Eng. Chem. Res. 2026, 65, 15071−15088

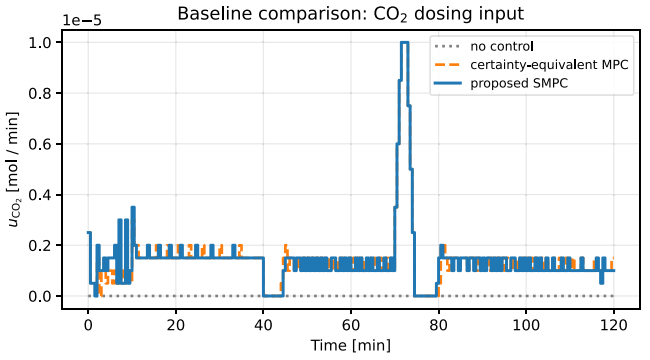

Figure 16. Baseline comparison of CO_2 dosing input between open-loop operation, certainty-equivalent MPC, and the proposed SMPC. The open-loop case uses no CO_2 dosing. The proposed SMPC propagates parametric uncertainty using PCE and performs uncertainty-aware regulation.

condition, whereas the post-transient metrics isolate controller performance after the unavoidable initial pH offset has been corrected.

The tracking metrics are computed from the ensemble mean pH trajectory $\bar{y}(t_k)$ as

$$\mathrm{RMSE} = \left(\frac{1}{N_T} \sum_{k \in \mathcal{T}} (\bar{y}(t_k) - y_{\mathrm{ref}}(t_k))^2 \right)^{1/2} \tag{47}$$

$$\mathrm{MAE} = \frac{1}{N_T} \sum_{k \in \mathcal{T}} |\bar{y}(t_k) - y_{\mathrm{ref}}(t_k)| \tag{48}$$

For realization r, the upper- and lower-bound violations are defined as

$$v_r^+(t_k) = \max\{0, y_r(t_k) - y_{\max}\} \tag{49}$$

$$v_r^-(t_k) = \max\{0, y_{\min} - y_r(t_k)\} \tag{50}$$

The integrated violation is computed as

$$J_{\mathrm{viol}} = \frac{1}{N_r} \sum_{r=1}^{N_r} \sum_{k \in \mathcal{T}} (v_r^+(t_k) + v_r^-(t_k)) \Delta t \tag{51}$$

Table 4 shows that SMPC improves constraint satisfaction under uncertain plant realizations. Over the full horizon, SMPC reduces the integrated upper pH violation from 1.809×10^{-1} to 1.245×10^{-1} and reduces the fraction of time outside the safety band from 3.817×10^{-2} to 1.598×10^{-2}. After the startup transient, the improvement is more pronounced: the integrated pH violation decreases from 7.742×10^{-2} for CE-MPC to 1.980×10^{-2} for SMPC, while the total CO_2 usage remains nearly unchanged. Thus, the benefit of SMPC is improved safety under modeled uncertainty, rather than lower nominal tracking error.

4. CONCLUSION

This work developed a control-oriented mechanistic model for buffer-free enzymatic urea hydrolysis that couples (i) pH-dependent urease kinetics with substrate and product inhibition, (ii) fast acid−base speciation closed by electroneutrality to compute pH, and (iii) gas−liquid mass transfer of NH_3 and CO_2 in a headspace. The model explains the characteristic open-loop pH rise as a thermodynamic consequence of the evolving TAN-DIC composition and provides an interpretable map from total species to pH. The resulting control interpretation is that CO_2 dosing regulates pH by steering the reacting mixture along a favorable TAN−DIC composition pathway, rather than by acting as a direct acid addition. To account for run-to-run variability in kinetic and transport parameters, we propagated parametric uncertainty using a nonintrusive PCE approach to obtain time-resolved pH statistics. Building on these predictions, we formulated a stochastic MPC scheme for CO_2 dosing that tracks a desired pH reference while enforcing input limits and probabilistic pH safety bounds. The numerical results show that the proposed controller can regulate pH near the urease optimal range and shift the full pH distribution into the desired operating window under uncertainty, rather than only stabilizing a nominal trajectory.

A limitation of the present study is that the SMPC controller is evaluated in closed-loop simulation rather than in a physical reactor. Therefore, the reported closed-loop results should be

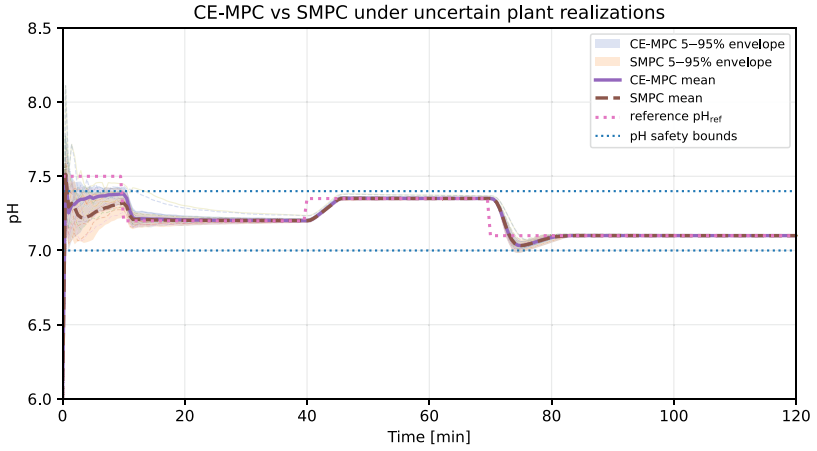

Figure 17. Closed-loop comparison between certainty-equivalent MPC and SMPC under the same uncertain plant realizations. Thin transparent curves show representative individual realizations, solid and dashed curves denote ensemble mean pH trajectories, and shaded regions denote empirical 5−95% envelopes. The dotted horizontal lines denote the pH safety bounds $7.0 \le \mathrm{pH} \le 7.4$. The CE-MPC envelope shows the uncertainty spread obtained when a nominal controller is applied to uncertain plant realizations, whereas the SMPC response reflects the chance-constraint tightening based on the propagated PCE moments.

https://doi.org/10.1021/acs.iecr.6c01013
Ind. Eng. Chem. Res. 2026, 65, 15071−15088

Table 4. Closed-Loop CE-MPC and SMPC Performance under Uncertain Plant Realizations[a]

Metric	full horizon		post-transient, $t \geq 2$ min	
	CE-MPC	SMPC	CE-MPC	SMPC
mean pH RMSE	1.134×10^{-1}	1.221×10^{-1}	5.619×10^{-2}	7.304×10^{-2}
mean pH MAE	3.187×10^{-2}	3.648×10^{-2}	2.417×10^{-2}	2.907×10^{-2}
mean maximum upper pH violation	1.648×10^{-1}	1.652×10^{-1}	3.005×10^{-2}	1.409×10^{-2}
mean integrated pH violation	6.869×10^{-1}	6.285×10^{-1}	7.742×10^{-2}	1.980×10^{-2}
mean integrated upper pH violation	1.809×10^{-1}	1.245×10^{-1}	7.439×10^{-2}	1.683×10^{-2}
fraction of time outside safety band	3.817×10^{-2}	1.598×10^{-2}	2.975×10^{-2}	6.329×10^{-3}
mean total CO_2 usage [mol]	1.410×10^{-4}	1.416×10^{-4}	1.385×10^{-4}	1.388×10^{-4}

[a]Metrics are reported over the full simulation horizon and after the startup transient, $t \geq 2$ min. The full-horizon metrics include the initial pH offset, whereas the post-transient metrics quantify controller performance after this initial correction phase.

Table 5. Kinetic Parameters from Qin and Cabral[7]

parameter	units	value	definition/role
k_0	mol NH_3 s^{-1} g_{urease}^{-1}	0.267	Arrhenius pre-exponential factor for the specific NH_3 formation rate (per g urease).
E_a	kJ mol^{-1}	29.1	activation energy in exp $(-E_a/RT)$.
K_M	mol L^{-1}	0.00256	Michaelis constant (substrate affinity) in the term $1 + K_M/[S]$.
K_S	mol L^{-1}	6.18	substrate inhibition constant in the term $1 + [S]/K_S$.
K_p(pH)	mol L^{-1}	$27.8 - 13.1\ pH + 2.32\ pH^2 - 0.183\ pH^3 + 0.0054\ pH^4$	pH-dependent product inhibition constant in the factor $1 + [P]/K_p$(pH).
$pK_{es,1}$	–	9.07 (25 °C); 9.43 (35 °C); 9.58 (40 °C)	pH-activity parameter (alkaline side of the window); $K_{es,1} = 10^{-pK_{es,1}}$ in mol L^{-1}.
$pK_{es,2}$	–	5.62 (25 °C); 5.28 (35 °C); 5.15 (40 °C)	pH-activity parameter (acidic side of the window); $K_{es,2} = 10^{-pK_{es,2}}$ in mol L^{-1}.
α	–	0.373 (25 °C); 0.489 (35 °C); 0.542 (40 °C)	empirical exponent shaping the pH-activity loss on the $K_{es,1}$ side.
β	–	0.564 (25 °C); 0.717 (35 °C); 0.769 (40 °C)	empirical exponent shaping the pH-activity loss on the $K_{es,2}$ side.

Table 6. Additional Definitions and Implementation Notes Used with the Kinetic Model

item	description
R	universal gas constant, $R = 8.314$ J mol^{-1} K^{-1}.
T	temperature (K), used in the Arrhenius term and/or temperature-dependent parameters.
pH, $[H^+]$	$[H^+] = 10^{-pH}$, with pH computed from the acid–base equilibria model.[1]
$[S]$	substrate concentration, $[S]$ = [UREA] (mol L^{-1}).
$[P]$	product concentration in the inhibition term; in this work, $[P] = [NH_3]$ (mol L^{-1}), computed from TAN speciation at the current pH.[7]
C_E	urease loading ($g_{urease}L^{-1}$) used to convert the specific rate to a volumetric rate: $r_{NH_3} = C_E\, \nu_{NH_3}$.
interpolation	for intermediate temperatures, tabulated parameters are obtained by linear interpolation in T between reported temperature points.

interpreted as a computational assessment of the uncertainty-aware control strategy. Experimental implementation would require real-time pH measurement, online state or parameter estimation, actuator calibration for CO_2 dosing, and validation of the gas–liquid transfer model under closed-loop operation. These steps are part of future work and are necessary before claiming experimental closed-loop performance.

A KINETIC-PARAMETER TABLES

Tables 5 and 6 provide the numerical values, definitions, and implementation notes for the kinetic parameters used throughout the paper.

AUTHOR INFORMATION

Corresponding Authors

Srimanta Santra – *Institute of Control Systems, Hamburg University of Technology, 21079 Hamburg, Germany*; Email: santrasrimanta7@gmail.com

Timm Faulwasser – *Institute of Control Systems, Hamburg University of Technology, 21079 Hamburg, Germany*; orcid.org/0000-0002-6892-7406; Email: timm.faulwasser@tuhh.de

Authors

Leandros Paschalidis – *Institute of Process Systems Engineering, Hamburg University of Technology, 21073 Hamburg, Germany*

Mirko Skiborowski – *Institute of Process Systems Engineering, Hamburg University of Technology, 21073 Hamburg, Germany*; orcid.org/0000-0001-9694-963X

Complete contact information is available at: https://pubs.acs.org/10.1021/acs.iecr.6c01013

Author Contributions

S.S.: Conceptualization, methodology, software, formal analysis, visualization, validation, and writing—original draft. L.P.: Writing—review. M.S.: Writing—review. T.F.: Conceptualization, methodology, supervision, and writing—review and editing.

Funding

This project is funded by the Deutsche Forschungsgemeinschaft (DFG, German Research Foundation)—SFB 1615 - 503850735.

Notes

The authors declare no competing financial interest.

REFERENCES

(1) Dittmer, K. R.; Paschalidis, L.; Ng-Brossard, C.; Ohde, D.; Liese, A.; Skiborowski, M. CO_2-Driven pH Control in the Enzymatic Hydrolysis of Urea: A Coupled Modeling−Experiment Approach. *Ind. Eng. Chem. Res.*, 2026.

(2) Nicolau, E.; Fonseca, J.; Rodríguez-Martínez, J.; Richardson, T.; Flynn, M.; Griebenow, K.; Cabrera, C. Evaluation of a Urea Bioelectrochemical System for Wastewater Treatment Processes. *ACS Sustainable Chem. Eng.* **2014**, *2*, 749−754.

(3) Urbańczyk, E.; Sowa, M.; Simka, W. Urea removal from aqueous solutions−a review. *J. Appl. Electrochem.* **2016**, *46*, 1011−1029.

(4) Yahya, M. N.; Gokcekus, H.; Orhon, D.; Keskinler, B.; Karagunduz, A.; Omwene, P. I. A Study on the Hydrolysis of Urea Contained in Wastewater and Continuous Recovery of Ammonia by an Enzymatic Membrane Reactor. *Processes* **2021**, *9*, No. 1703.

(5) Krajewska, B. Ureases I. Functional, catalytic and kinetic properties: A review. *J. Mol. Catal. B:Enzym.* **2009**, *59*, 9−21.

(6) Mobley, H. L. T.; Island, M. D.; Hausinger, R. P. Molecular Biology of Microbial Ureases. *Microbiol. Rev.* **1995**, *59*, 451−480.

(7) Qin, Y.; Cabral, J. M. S. Kinetic studies of the urease-catalyzed hydrolysis of urea in a buffer-free system. *Appl. Biochem. Biotechnol.* **1994**, *49*, 217−240.

(8) Hu, G.; Chen, J.; Fang, Q.; Smith, M. A.; Broomfield, J. A. Base-Catalyzed Feedback in the Urea−Urease Reaction. *J. Phys. Chem. B* **2010**, *114*, 14059−14063.

(9) Stumm, W.; Morgan, J. J. *Aquatic Chemistry: Chemical Equilibria and Rates in Natural Waters*, 3rd ed.; Wiley-Interscience, 1995.

(10) Tchobanoglous, G.; Stensel, H. D.; Tsuchihashi, R.; Burton, F. L.; Metcalf & Eddy, Inc. *Wastewater Engineering: Treatment and Resource Recovery*, 5th ed.; McGraw-Hill Education, 2014.

(11) Zeebe, R. E.; Wolf-Gladrow, D. *CO2 in Seawater: Equilibrium, Kinetics, Isotopes*, Elsevier Oceanography Series; Elsevier: Amsterdam, 2001; Vol. *65*.

(12) Danckwerts, P. V. *Gas-Liquid Reactions*; McGraw-Hill Book Company: New York, 1970.

(13) Cussler, E. L. *Diffusion: Mass Transfer in Fluid Systems*, 3rd ed.; Cambridge University Press, 2009.

(14) Sander, R. Compilation of Henry's law constants (version 4.0) for water as solvent. *Atmos. Chem. Phys.* **2015**, *15*, 4399−4981.

(15) Levenspiel, O. *Chemical Reaction Engineering*, 3rd ed.; Wiley, 1999.

(16) Fogler, H. S. *Elements of Chemical Reaction Engineering*, 5th ed.; Prentice Hall, 2016.

(17) Wiener, N. The homogeneous chaos. *Am. J. Math.* **1938**, *60*, 897−936.

(18) Cameron, R. H.; Martin, W. T. The orthogonal development of non-linear functionals in series of Fourier-Hermite functionals. *Ann. Math.* **1947**, *48*, 385−392.

(19) Xiu, D.; Karniadakis, G. E. The Wiener−Askey polynomial chaos for stochastic differential equations. *SIAM J. Sci. Comput.* **2002**, *24*, 619−644.

(20) Ghanem, R. G.; Spanos, P. D. *Stochastic Finite Elements: A Spectral Approach*; Courier Corporation: New York, 2003.

(21) Xiu, D.; Karniadakis, G. E. Modeling uncertainty in flow simulations via generalized polynomial chaos. *J. Comput. Phys.* **2003**, *187*, 137−167.

(22) Najm, H. N. Uncertainty quantification and polynomial chaos techniques in computational fluid dynamics. *Annu. Rev. Fluid Mech.* **2009**, *41*, 35−52.

(23) Mühlpfordt, T.; Roald, L.; Hagenmeyer, V.; Faulwasser, T.; Misra, S. Chance-constrained AC optimal power flow: A polynomial chaos approach. *IEEE Trans. Power Syst.* **2019**, *34*, 4806−4816.

(24) Mühlpfordt, T.; Findeisen, R.; Hagenmeyer, V.; Faulwasser, T. Comments on truncation errors for polynomial chaos expansions. *IEEE Control Syst. Lett.* **2018**, *2*, 169−174.

(25) Dodson, M.; Parks, G. T. Robust aerodynamic design optimization using polynomial chaos. *J. Aircraft* **2009**, *46*, 635−646.

(26) Pan, G.; Ou, R.; Faulwasser, T. On a stochastic fundamental lemma and its use for data-driven optimal control. *IEEE Trans. Autom. Control* **2023**, *68*, 5922−5937.

(27) Xiu, D. Efficient collocational approach for parametric uncertainty analysis. *Commun. Comput. Phys.* **2007**, *2*, 293−309.

(28) Nobile, F.; Tempone, R.; Webster, C. G. A sparse grid stochastic collocation method for partial differential equations with random input data. *SIAM J. Num. Anal.* **2008**, *46*, 2309−2345.

(29) Mesbah, A.; Streif, S.; Findeisen, R.; Braatz, R. D. Stochastic nonlinear model predictive control with probabilistic constraints. *Am. Control Conf.* **2014**, 2413−2419.

(30) Paulson, J. A.; Mesbah, A. Nonlinear Model Predictive Control with Explicit Backoffs for Stochastic Systems under Arbitrary Uncertainty. *IFAC-PapersOnLine* **2018**, *51*, 523−534.

(31) Nemirovski, A.; Shapiro, A. Convex approximations of chance constrained programs. *SIAM J. Optim.* **2007**, *17*, 969−996.

https://doi.org/10.1021/acs.iecr.6c01013
Ind. Eng. Chem. Res. 2026, 65, 15071−15088